Oncogenic mutations of *PIK3CA* lead to increased membrane recruitment driven by reorientation of the ABD, p85 and C-terminus

Harish Ranga-Prasad[1], Meredith L Jenkins[1], Matthew AH Parson[1], Manoj K Rathinaswamy[1], John E Burke[1,2%]

[1]Department of Biochemistry and Microbiology, University of Victoria, Victoria, British Columbia, V8W 2Y2, Canada

[2]Department of Biochemistry and Molecular Biology, The University of British Columbia, Vancouver, British Columbia V6T 1Z3, Canada

Running title: Dynamic allosteric changes upon activation of oncogenic *PIK3CA*

[%]To whom correspondence should be addressed: John E. Burke

Tel: 1-250-721-8732, email: jeburke@uvic.ca

Keywords: PI3K, PI3Kα, PIK3CA, p110α, PIK3R1, phosphoinositide 3-kinase, hydrogen exchange, HDX-MS, protein dynamics, allostery.

Abstract

PIK3CA encoding the phosphoinositide 3-kinase (PI3K) p110α catalytic subunit is frequently mutated in cancer. The mechanisms underlying PI3K activation on membranes, and how oncogenic mutations distributed throughout p110α increase kinase activity is undefined. Using a synergy of biochemical assays and hydrogen deuterium exchange mass spectrometry (HDX-MS), we reveal unique regulatory mechanisms underlying PI3K activation. Engagement of p110α on membranes leads to disengagement of the ABD domain of p110α from the catalytic core, and the C2 domain from the iSH2 domain of the p85 regulatory subunit. PI3K activation also requires reorientation of the C-terminus, with mutations that alter the inhibited conformation of the C-terminus increasing membrane binding. Mutations at the C-terminus (M1043I/L, H1047R, G1049R, and N1068KLKR) activate p110α through distinct mechanisms, with this having important implications for mutant selective inhibitor development. This work reveals unique mechanisms underlying oncogenic mutants activate PI3K and explains how double mutants can synergistically increase PI3K activity.

Introduction

Activating mutations in the gene *PIK3CA*, which encodes the class IA phosphoinositide 3-kinase (PI3K) catalytic subunit p110α are among the most common mutations across human cancers[1–4]. Class I PI3Ks are composed of four isoforms (class IA [p110α, p110β, p110δ] and class IB [p110γ]), which together generate the lipid second messenger phosphatidylinositol 3,4,5 trisphosphate (PIP_3) downstream of multiple cell surface receptors, including receptor tyrosine kinases (RTKs), G-protein coupled

receptors (GPCRs), and Ras superfamily GTPases. PIP_3 recruits multiple effectors, including kinases and regulators of G protein signalling which play critical roles in regulating growth, survival, proliferation, and metabolism[5–7].

PI3Kα is a hetero-dimer composed of a p110α catalytic subunit and a p85 regulatory subunit, of which there are 5 isoforms: p85α, p55α and p50α (encoded by *PIK3R1*), p85β (encoded by *PIK3R2*) and p55γ (encoded by *PIK3R3*). The class IA regulatory subunits play three key roles in regulating class IA PI3Ks: they stabilize and inhibit the p110 catalytic subunits[8,9], and they allow for activation through the direct engagement of the nSH2 and cSH2 domains of regulatory subunits with pYXXM motifs in RTKs[10]. In unstimulated cells, the p110α protein is kept in an inactive and stable cytosolic configuration due to its interactions with the regulatory subunit, with full activation and membrane recruitment of the PI3Kα complex requiring binding to both GTP loaded Ras, and engagement of both the nSH2 and cSH2 of regulatory subunits by bis-phosphorylated pYXXM motifs present in RTKs and their adaptors[11–13]. However, the full molecular mechanisms underpinning membrane binding and class IA PI3K activation are still unknown.

Extensive biochemical and biophysical studies have revealed how p110α is inhibited by regulatory subunits[14–20]. The p110α catalytic subunit is composed of five domains (adaptor binding domain (ABD), Ras Binding domain (RBD), C2, helical and a bi-lobal kinase domain)[14,21] (Fig. 1A). The RBD, C2, helical, and kinase domains together form the catalytic core of PI3Ks, which is conserved through the class I, II, and III PI3Ks[22,23]. The ABD of class IA PI3Ks binds irreversibly to the iSH2 coiled coil domain present in all class IA regulatory subunits[15], and also forms an inhibitory intra-subunit

interface with the N-lobe of the kinase domain (Fig. 1A,1B). The iSH2 also makes inhibitory contacts with the C2 and activation loop of the kinase domain[16,24]. The nSH2 domain of regulatory subunits binds reversibly to the C2, helical and kinase domains[15,17], with these contacts broken when the nSH2 binds to pYXXM motifs[19]. The cSH2 of regulatory subunits is strictly required for high affinity association with bis-phosphorylated receptors and their adaptors[11], and in p110β and p110δ forms an inhibitory interface with the kinase domain, however, this interaction is either absent or transient in p110α[25,26]. Recently Cryo-EM analysis of p110α bound to p85α showed that upon binding to phosphopeptides there appeared to be complete disengagement of the ABD and regulatory subunit from the catalytic core[27], which was not fully supported by previous HDX-MS analysis of phosphopeptide binding[16,19]. However, disengagement of the catalytic core from the ABD and regulatory subunits is consistent with HDX-MS results studying PI3K membrane binding[12].

The *PIK3CA* and *PIK3R1* genes encoding p110α and p85α are both frequently mutated in human cancers[1,2,28]. The majority of mutations lead to amino acid substitutions (Fig. 1C)[29], although, more complex insertions and deletions also occur[30]. Oncogenic transformation by p85α mutations is driven by activation of the p110α isoform[31]. For p110α the most frequent mutations are located at two hot spots located at the helical-nSH2 interface (E542K, E545K) and the C-terminus of the kinase domain (H1047R) (Fig. 1B). The E545K disrupts the nSH2-helical interface[15] while H1047R alters the membrane binding surface of the kinase domain (Fig. 1D.1E)[17]. However, there also are relatively high frequency mutations at the ABD-kinase interface, the ABD-RBD linker, the C2-iSH2/C2-nSH2 interfaces, the putative membrane interface of the N-lobe with

membranes, and in a region of the kinase domain C-terminal to the activation loop, referred to as the regulatory motif (Fig. 1C)[32]. We have previously found that oncogenic mutations mimicked and enhanced conformational changes observed in the catalytic cycle of WT PI3Kα[16], with different mutants showing unique conformational changes. Different *PIK3CA* mutations activating lipid kinase activity through unique mechanisms is supported by the discovery of tumours harbouring double *PIK3CA* mutations *in cis*, with these tumours showing enhanced sensitivity to PI3K inhibition[33].

Here, using a combination of hydrogen deuterium exchange mass spectrometry (HDX-MS) and kinase/membrane binding assays, we provide a molecular model for how oncogenic mutants in p110α activate both kinase activity and membrane binding. This has revealed the critical role of disengagement of the inhibitory contacts of the ABD domain and the p85 regulatory subunit, as well as the importance of reorganisation of the membrane binding C-terminus in PI3K activation. Intriguingly, mutations at the C-terminal tail activate PI3K through distinct molecular mechanisms and provide unique insight into how this might be utilised in mutant selective inhibitor design. Overall, this work provides unique insight into the molecular mechanisms mediating PI3K activation by oncogenic mutations.

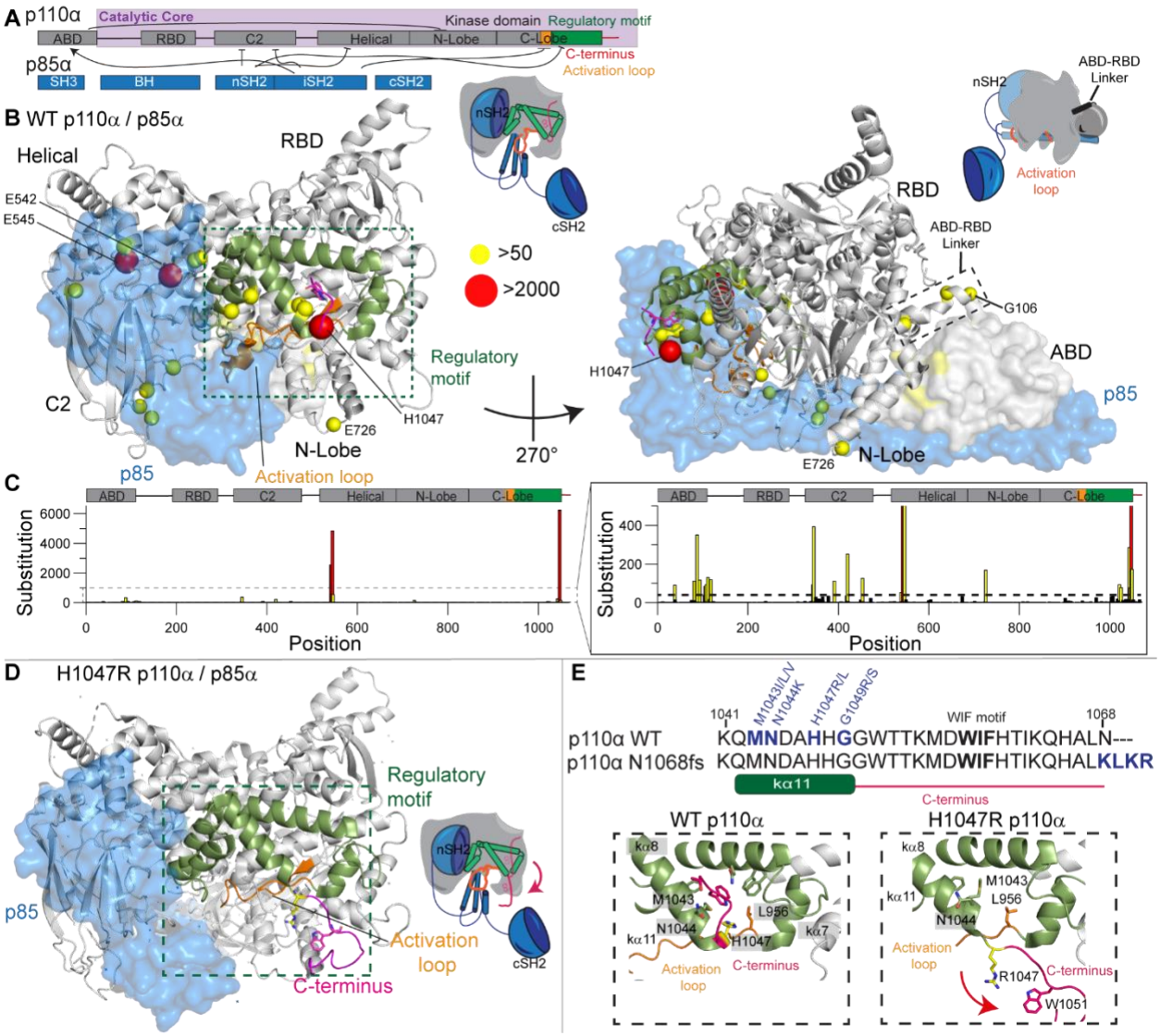

Fig 1. Structure of p110α/p85α and location of *PIK3CA* oncogenic mutations

A. Domain schematic of both p110α/p85α, with the catalytic core, activation loop, regulatory motif, and C-terminus of p110α annotated.

B. Oncogenic mutations in p110α mapped on the structure of WT p110α/p85α (PDB: 4OVU[34]). The frequency of oncogenic mutations is colored according to the legend, with features colored according to the domain schematic in panel A. Cartoons of the two views of PI3K highlighting these features are shown to the right of each structural model. These same cartoon views are used to map all further HDX-MS data.

C. Frequency of mutations across the primary sequence of *PIK3CA* from the **C**atalog **o**f **S**omatic **M**utations **i**n **C**ancer (COSMIC) database (data from January 2022)[35].

D. C-terminus in H1047R adopts a unique confirmation compared to WT (PDB: 3HHM)[17]. Features are colored the same as in panel B.

E. Orientation of the C-terminus in the WT (PDB:4OVU) and H1047R (PDB:3HHM) crystal structures. The relative positioning of additional oncogenic mutants (M1043I/L, N1044K, G1049R/S) are indicated. The sequence of the C-terminus is shown, with mutants colored blue, and the membrane binding WIF motif in bold[36]. The sequence of one of the recently discovered frameshift mutants (N1068KLKR)[30] is shown.

Results

To investigate the role of ABD/p85 in controlling the enzyme activity, we needed a construct that allowed us to interrogate the dynamic effects of full ABD disengagement. We engineered and purified the catalytic core of p110α (106-1068, referred to as ΔABD) along with the full-length complex of p110α-p85α (full set of all constructs purified in this manuscript shown in Fig. S1, and SDS-page gels in Fig. S2). Attempts to purify the ΔABD construct were unsuccessful, and we were only able to successfully purify this construct when it contained a kinase dead mutation (D915N). To validate that the D915N p110α construct did not cause any significant changes in protein conformation or membrane binding, we carried out HDX-MS experiments on WT and kinase dead p110α-p85α complexes bound to a PDGFR bis-phosphorylated pY peptide (referred to going forward as pY) composed of PDGFR residues 735–767 with phosphorylation present at Y740 and Y751 in the presence and absence of membrane vesicles (5% PIP_2, 30% PS, 65% PE, referred to afterwards as PIP_2/PS/PE). HDX-MS is a technique that measures the

exchange rate of amide hydrogens, and as the rate is dependent on the presence and stability of secondary structure, it is an excellent probe of protein conformational dynamics, and we have extensively used it to study PI3K activation[11,12,16,19,25]. There were no significant changes in conformation in the kinase dead p110α compared to wild-type, and both had equivalent membrane binding to lipid membranes (Fig. S3).

We carried out HDX-MS experiments to identify conformational changes that occur in the catalytic core of p110α upon removal of the ABD and p85α regulatory subunit. We compared H/D exchange differences in the core for both ΔABD and the full-length complex of p110α-p85α. The full details of HDX-MS data processing are in Table S1, with all raw HDX-MS data for all time points available in the source data. For the ΔABD construct there was significantly increased exchange (for all HDX-MS experiments this is defined as differences at any time point >5%, >0.4 Da, and a p-value less than 0.01 for a two-tailed t-test) in the ABD-RBD linker (114-119), C2 domain (347-355 and 444-475), helical domain (524-551), N-lobe of the kinase domain (691-697, 735-744), the activation loop (930-937) and the C-lobe of the kinase domain (1002-1013) (Fig. 2A-D,S4A-B). All significant differences in the catalytic core of p110α were in regions that were either in contact with ABD or p85α. This dataset allowed us to compare changes to those we previously observed upon membrane recruitment by both pY, and membrane bound Ras of the full length p110α-p85α complex (Fig. 2B)[12]. Intriguingly, we find that the region of the ABD-RBD linker in contact with the ABD domain (114-119) had similar increases in exchange between WT p110α-p85α and either the ΔABD construct or upon pY/HRas mediated membrane recruitment (Fig. 2D). There is a small increase in exchange in this region upon pY binding alone, but this was minor compared to the effect upon membrane

binding[16,19]. The increase in region 114-119 was greater when bound to pY/HRas membranes compared to pY mediated membrane binding alone, suggesting this increase is dependent on the amount of membrane binding (Fig. 2D). This is also the case for increases in exchange observed upon membrane binding in the N-terminal and C-terminal ends of the iSH2 domain that are in contact with the C2 domain (470-476, 556-570, Fig S4E), showing the clear link between increases in the ABD-RBD linker and at the C2-iSH2 interface. Overall, this data supports that disengagement of the ABD and p85 subunit from the p110α catalytic core occurs upon membrane binding. An important note is that this data does not support complete dissociation of the p110-p85 complex (due to the extremely high affinity interaction of the ABD to the iSH2), but instead the ABD-p85 becoming mobile relative to the p110α catalytic core.

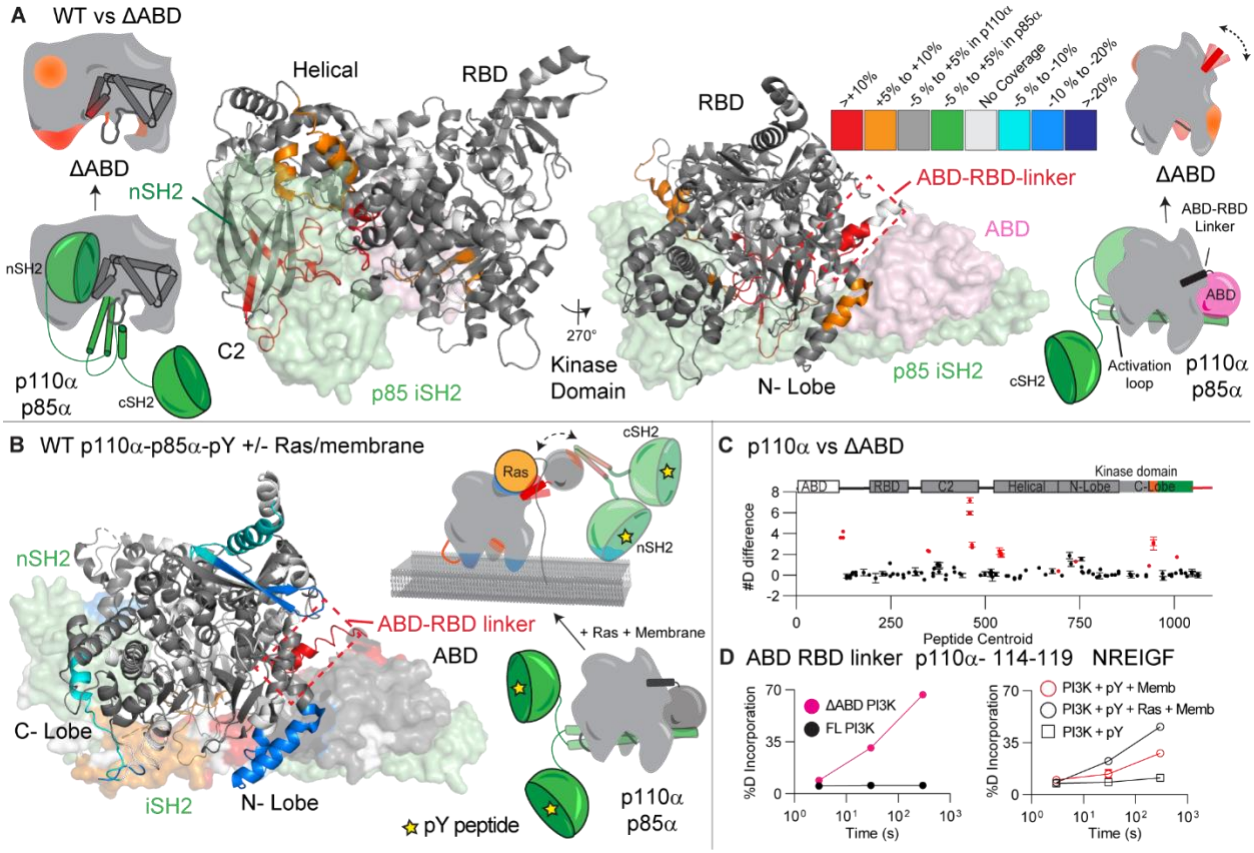

Fig 2. Conformational changes in ΔABD p110α compared to full length p110α- p85α, and comparison to changes upon pY/Ras membrane recruitment

A. Peptides in p110α that showed significant differences in HDX (greater than 0.4 Da and 5% difference, with a two tailed t-test p<0.01) between the catalytic core and the full-length complex are mapped on the structure of p110α-p85α complex (PDB: 4OVU) according to the legend. The regions of the ABD (pink) and p85 (green) that are missing in the ΔABD construct are shown as a surface. Cartoon models representing the differences between states are shown next to the structures.

B. Peptides in p110α that showed significant differences in both p110α and p85α between free (with pY) and membrane-bound (pY, membrane Ras) (data from Siempelkamp et al JBC, 2017[12]) are mapped onto the structure of p110α-p85α (PDB:4OVU) according to the legend. A more extensive set of peptides are shown in Fig S4.

C. The number of deuteron difference for all peptides analyzed over the entire deuterium exchange time course for ΔABD p110α compared to full length p110α- p85α. Peptides colored in red are those that had a

significant change (greater than 0.4 Da and 5% difference at any timepoint, with a two tailed t-test $p<0.01$). Error bars are S.D. (n=3).

D. Selected p110α peptide in the ABD-RBD linker that showed increases in exchange in ΔABD p110α compared to full length p110α-p85α (left), and upon membrane binding of full length PI3K (right, data from [12]). Error bars are S.D. (n=3), with most smaller than the size of the point. A more extensive set of peptides are shown in Fig. S4, with the full list of all peptides and their deuterium incorporation in the source data file.

Enhanced membrane binding of ΔABD p110α

Our hypothesis that disengagement of the ABD regulatory p85α subunit is required for membrane binding suggested that there should be differential membrane binding of the ΔABD p110α compared to full length p110α/p85α. We used protein-lipid fluorescent resonance energy transfer (FRET) assays (Fig. 3A) to compare membrane recruitment of ΔABD p110α to full length p110α-p85α in the presence and absence of 1 μM pY. This assay was carried out on two different lipids: one roughly mimicking the plasma membrane (5% PIP_2, 10% Dansyl PS, 15 % PS, 40% PE, 15% PC, 10% cholesterol, and 5% sphingomyelin, Fig. 3B) and another optimised for maximal PI3K recruitment (5% PIP_2, 10% Dansyl-PS, 25 % PS and 60 % PE, Fig. S4E). While pY was required for robust binding of full length p110α-p85α, it was dispensable for ΔABD p110α association, which is expected due to the lack of SH2 domains required for pY binding (Fig. 3B). The ΔABD p110α showed increased membrane recruitment for both lipid mixtures compared to the pY activated p110α/p85α complex.

Defining the membrane binding surface of ΔABD p110α

We have extensively characterised the membrane binding of the p110α/p85α complex using HDX-MS, however, the disengagement of the ABD and p85 from the catalytic core has likely complicated the analysis of membrane binding regions. We carried out HDX-MS experiments of ΔABD p110α in the presence and absence of 5% PIP_2/PS/PE membranes to fully understand the molecular underpinnings of p110α membrane binding. We observed protection in the ABD-RBD linker (114-119), C2 (343-355), N-lobe kinase domain (713-734,735-744,799-811 and 850-859), Activation loop (930-961) and the C-terminus of the C-lobe kinase domain (1039-1055 and 1056-1068) (Fig. 3A-C). Overall, this supports a model where p110α binds membrane at a surface composed of the C2 domain, the kα1-kα2 helices (720-744) and the 859-872 region of the N-lobe, the activation loop, along with the C-terminal tail. Intriguingly, the kα1-kα2 helices in the N-lobe interact with the ABD, and the 343-355 region of the C2 domain binds the N+C termini of the iSH2 domain, which provides a putative molecular explanation for why disengagement of the ABD and p85 leads to increased membrane association.

When comparing our data to the full set of missense oncogenic mutations in the ABD, ABD-RBD linker, C2, helical, and the N-lobe of the kinase domain we find that all mutations found in >30 tumours except one (E726K) are located at either the ABD or p85 interfaces. We had previously observed that mutations in the ABD-RBD linker caused similar conformational changes to those located at the C2-iSH2 interface, with this being explained by both mutations leading to disengagement of the ABD and p85 from the catalytic core[16].

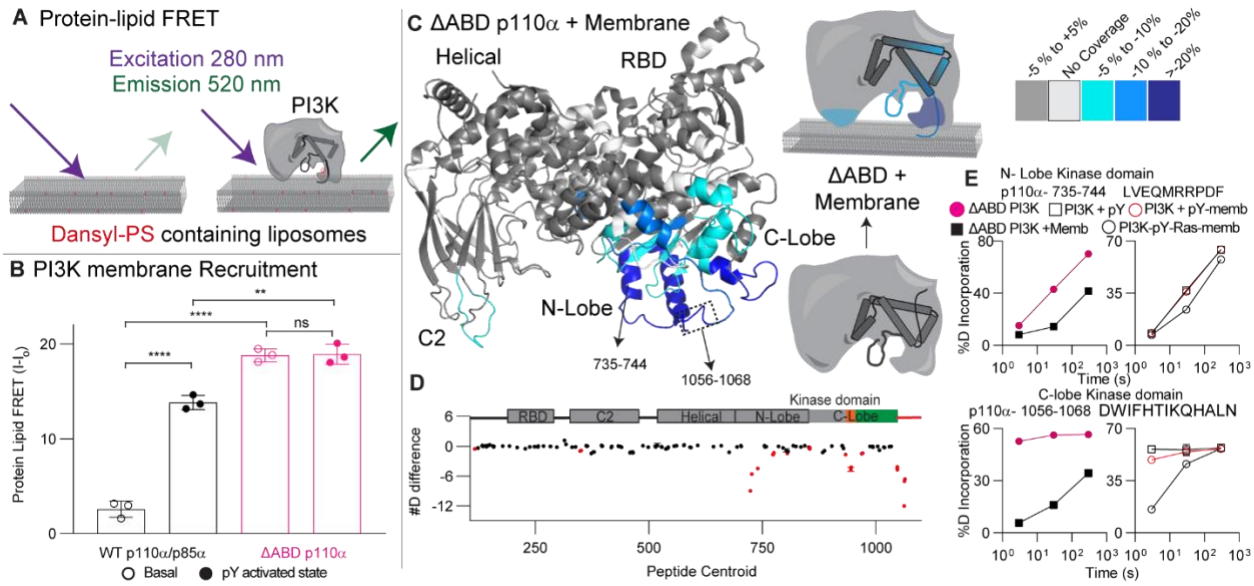

Fig 3. Enhanced membrane binding of ΔABD p110α compared to full length p110α/p85α, and mapping of the p110α membrane binding interface

A. Cartoon schematic describing the protein-lipid FRET assay, where tryptophan's in the protein are excited at 280 nm, with emission at 350 nm, which upon membrane binding can excite the dansyl moiety in dansyl phosphatidylserine lipids, leading to emission at 520 nm.

B. Protein-lipid FRET measurements of membrane recruitment for both ΔABD and full-length p110α/p85α complex under basal and pY activated conditions on PM mimic liposomes containing 5% PIP_2, 10% Dansyl PS, 15 % PS, 40% PE, 10% cholesterol, 15% PC and 5% SM (error bars are S.D., n=3). Experiments were carried out with 1 µM pY, 0.5 µM PI3K, and 33.33 µg lipid vesicles. Two tailed p-values represented by the symbols as follows: ****<0.0001; **<0.01; n.s.>0.05.

C. Peptides in ΔABD p110α that showed significant differences in HDX (greater than 0.4 Da and 5% difference, with a two tailed t-test p<0.01) upon binding to 100 nm extruded 5% PIP_2/PS/PE vesicles were mapped onto the catalytic core of p110α (PDB: 3HHM) according to the legend.

D. The number of deuteron difference for all peptides analyzed over the entire deuterium exchange time course for ΔABD p110α upon binding membranes. Peptides colored in red are those that had a significant change (greater than 0.4 Da and 5% difference at any timepoint, with a two tailed t-test p<0.01). Error bars are S.D. (n=3).

E. Selected p110α peptide in the kinase domain that showed decreases in exchange in ΔABD p110α upon binding membranes (left), and pY or pY-Ras mediated membrane binding of full length p110α-p85α (right, data from[12]). A more complete set of peptides are shown in Fig S4, with the full list of all peptides and their deuterium incorporation in the source data file.

Role of the conformation of the C-terminus of the kinase domain in PI3K activation

While the disengagement of the ABD and p85 being involved in membrane binding provides a molecular rationale for activation by oncogenic mutations in the ABD, C2, and helical domains, it does not fully explain the molecular mechanism of mutations in the C-lobe of the kinase domain. Our previous HDX-MS analysis of the kinase domain mutant, H1047R, showed increased exposure throughout regions of the N-lobe and C-lobe of the kinase domain, with this resulting in a dramatic increase in membrane binding[16]. Since this study there have been an extensive number of additional p110α/p85α structures solved using Cryo Electron microscopy and X-ray crystallography. This allowed us a new resource to possibly interpret our original data in the context of new structural information.

The highest resolution structures of p110α-p85α solved to date are 4JPS (2.20 Å)[37], 4WAF (2.39 Å)[38], 5FI4 (2.50 Å)[39] and 4OVU (2.96 Å)[34]. These structures all showed a novel orientation of the C-terminus of the kinase domain that was absent in the original p110α/p85α structure (2RD0, 3.03 Å)[14]. In high resolution structures the C-terminus of p110α makes extensive contacts with helices that make up the regulatory motif (kα8 and kα11) and sits on top of the C-terminus of the activation loop (Fig. 1E). One of the primary interactions is an extensive interface between Trp1051 of the C-terminus and His1047 as well as hydrophobic residues lining kα8 and kα11 of the kinase domain (Met1043, Phe977,980 and 1039). This region is also in contact with Leu956 in the C-terminal end

of the activation loop. This orientation positions the membrane binding WIF motif (residues 1057-1059) distant from the membrane binding interface. When comparing these WT p110α structures to the H1047R crystal structure (3HHM), there is a significant reorganisation of the C-terminus, with all contacts between the C-terminus and kα8 and kα11 disrupted, and the WIF motif oriented at the putative membrane surface (Fig. 1D)[17]. This is putatively mediated by mutation of His1047 preventing the C-terminal interaction due to the increased size of the Arg residue compared to His preventing formation of the inhibitory C-terminal conformation (Fig. 1E) and orienting the lipid binding WIF motif at the membrane interface.

Biochemical analysis of oncogenic mutations in the inhibitory C-terminus

To understand the regulatory mechanisms underlying the inhibitory interface with the C-terminus we analysed the most frequent oncogenic mutants that occur at or near this interface. While H1047R/L is the most frequent mutation (>6000 from the COSMIC database), there are multiple frequent missense mutations in this region, including M1043L/I/V (>300), G1049R/S (>150), and N1044K/S (>80). In addition, we analyzed an activating frameshift variant that alters the C-terminus by replacing the terminal N with a KLKR extension, which was recently identified in tumour samples (N1068KLKR, referred to afterwards as N1068fs)[30]. To understand if these mutants were activated in a similar way to H1047R, we purified the four p110α mutant complexes (M1043L, H1047R, G1049R, and N1068fs) all bound to full length p85α.

Initial attempts to characterise the lipid kinase activity of these mutants using an assay that measures the generation of ADP (Fig. 4A) as a surrogate for PIP_3 production

revealed striking differences in basal ATPase activity in the absence of membranes (described in more detail below), preventing the use of this assay approach. Due to this complication, we characterised the lipid kinase activity using an assay that measures the consumption of PIP_2 through altered recruitment of a high specificity PIP_2 fluorescent sensor consisting of ENTH domain (Fig. 4B)[40]. Lipid kinase assays on PIP_2/PS/PE vesicles showed that all mutants were significantly activated over wild type p110α both in the absence and presence of pY, with ~10-50-fold increased activity (Fig. 4D+E). All constructs showed a ~4-7-fold activation upon pY binding (Fig. S5). We also characterised the intrinsic ATPase activity of each p110α mutant (Fig. 4C) in solution. While this assay does not measure biologically relevant PI3K activity, it can measure intrinsic difference in PI3K activity independent of membrane binding. Where assays on PIP_2 membrane substrates showed similar activation for all mutants compared to WT, the basal ATPase assays showed distinct differences between the mutants. Both H1047R and G1049R had ~4-fold increased ATPase activity compared to WT, with ~9-fold increased ATPase activity compared to WT when both were activated by pY (Fig. 4C). However, M1043L and the N1068fs mutants showed ATPase activity that was indistinguishable from WT both in the presence and absence of pY. This suggested a possible conformational difference between G1049R and H1047R compared to M1043L and N1068fs.

For these mutants, we had difficulty in obtaining sufficient yield of the proteins for extensive biophysical analysis. To circumvent this, we used the kinase dead variants to characterize their membrane binding using protein-lipid FRET using both PM mimic and optimised binding lipids. Membrane binding was enhanced for mutants upon addition of

pY, with greater binding for the optimised lipids over the PM mimic (Fig. S6D). A p110α construct lacking the C-terminus (1-1048, referred to afterwards as ΔCter) showed very little membrane binding as indicated by the absence of a FRET signal, which is expected due to the loss of the WIF membrane binding motif. H1047R, G1049R, and N1068fs all showed significantly increased membrane binding over WT both with and without pY (Fig. 4F), while the M1043 mutant only showed a slight increase in membrane binding without pY for the PM mimic vesicles (Fig. 4F).

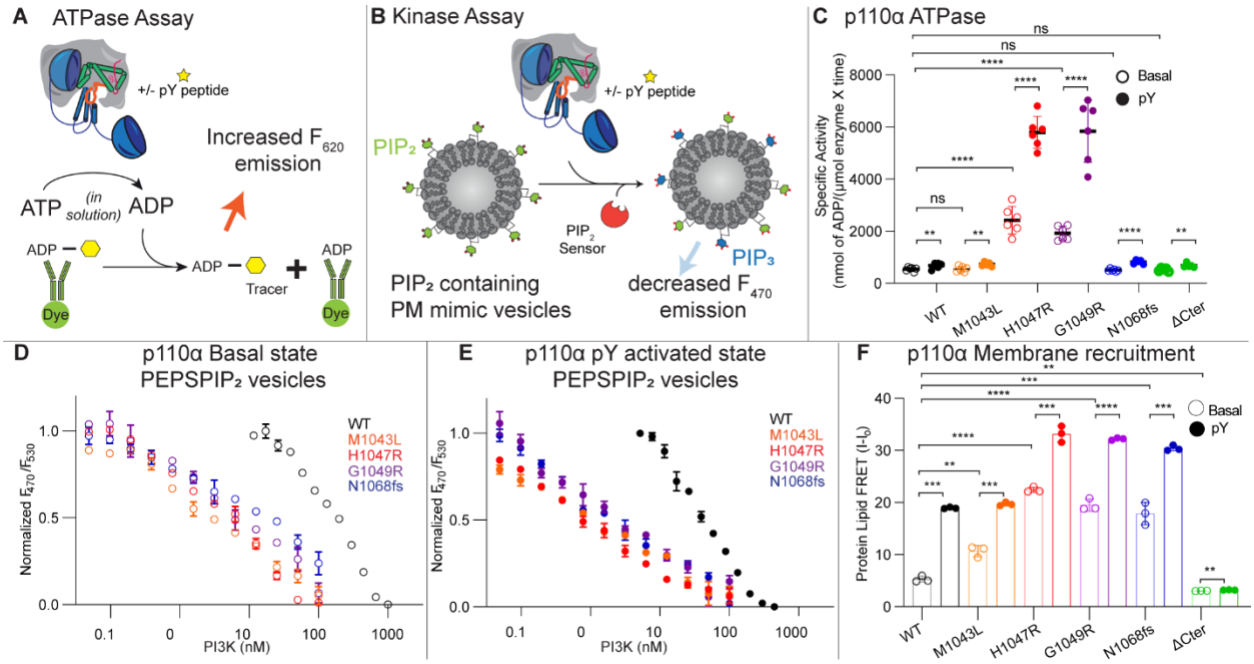

Fig 4. Biochemical analysis of C-terminal *PIK3CA* mutations and their effect on membrane binding, lipid kinase and ATPase assays

A. Cartoon schematic describing of ATPase assay measuring ADP production from ATP.

B. Cartoon schematic describing the protein kinase assay with a fluorescent ENTH domain that recognises PIP_2. PIP_2 is depleted as PI3K generates PIP_3, leading to decreased emission at 470 nm.

C. ATPase assay performed with different p110α constructs in solution (error bars are S.D., n=6). Experiments were performed with 0.05 to 0.3 µM PI3K, 1 µM pY, and 100 µM ATP in the absence of lipid

vesicles. Two tailed p-values represented by the symbols are as follows: ****<0.0001, ***<0.001; **<0.01; *<0.05; n.s.>0.05

D. Lipid kinase assay performed with different p110α constructs under basal state. Experiments were performed with1 μM ATP, 0.4 X 10^{-3} to 0.8 μM PI3K, and 1 mg/ml of PIP_2/PS/PE vesicles (5% PIP_2, 30% PS, 65% PE). All mutants showed to 10-50-fold increase in kinase activity. (Error bars are SD, n=3)

E. Lipid kinase assays on p110α constructs in the presence of 1 μM bis-phosohorylated PDGFR peptide (pY) (error bars are SD, n=3)

F. Protein-Lipid FRET assay performed with different p110α constructs under basal and pY activated states on PM mimic liposomes containing 5% PIP_2, 10% Dansyl PS, 15 % PS, 40% PE, 10% cholesterol, 15% PC and 5% SM. Experiments were carried out at saturating concentrations of PI3K (1μM) and 33.33 μg/ml of lipid vesicles (error bars are S.D., n=3).

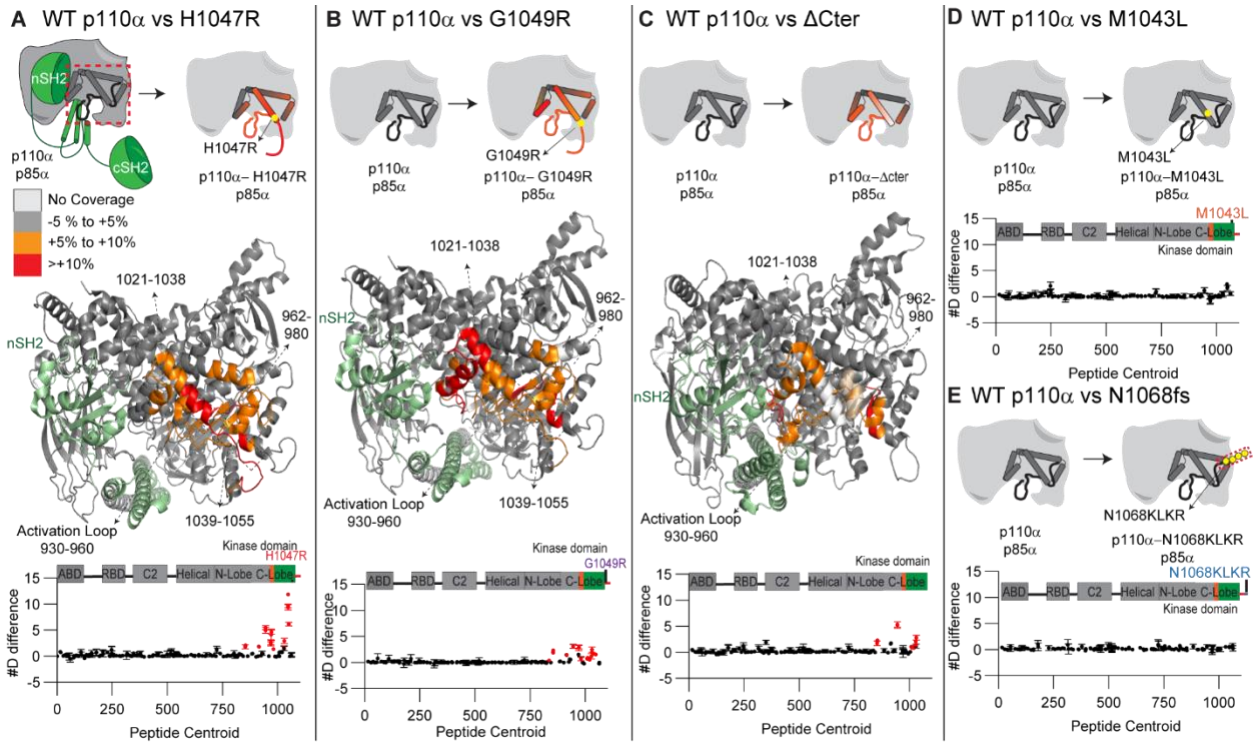

Fig 5. Structural difference between various c-terminal mutants of p110α compared to WT p110α/p85α, and mapping of the p110α membrane binding interface

A-C. HDX comparing p110α/p85α WT vs H1047R (**A**), G1049R (**B**) and ΔCter (1-1048) (**C**). Significant differences in deuterium exchange are mapped on to the structure of p110α/p85α H1047R according to the

legend (PDB: 3HHM (A+B) and 4OVU (C)). The graph of the #D difference in deuterium incorporation for p110α in each experiment is shown below, with each point representing a single peptide. Peptides colored in red are those that had a significant change in the mutants (greater than 0.4 Da and 5% difference at any timepoint, with a two tailed t-test p<0.01). Error bars are S.D. (n=3).

D-E. HDX comparing p110α/p85α WT vs M1043L (D) and N1068fs (E). The graph of the #D difference in deuterium incorporation for p110α in each experiment is shown below, with each point representing a single peptide. For all panels the HDX-MS data for p85 subunits is shown in Fig S6, along with representative peptides showing significant changes. The full HDX-MS data is available in the source data.

Conformational changes in oncogenic mutations C-terminus of the kinase domain

To test if C-terminal mutations worked by disrupting the inhibitory interaction with the C-terminus, we carried out HDX-MS studies on six constructs of full length p110α (WT, M1043L, H1047R, G1049R, 1068fs, and ΔCter), all bound to full length p85α. The use of the ΔCter construct allowed for a direct comparison of removal of the C-terminus, versus a possible reorientation upon oncogenic mutation. We used kinase active M1043L, H1047R, G1049R, and a kinase dead variant of N1068fs for this comparison.

HDX-MS experiments were carried out for 4-5 timepoints of exchange (3 s at 1°C, 3, 30, 300, and 3000 s at 20°C) for each complex. The full set of all peptides analysed for both p110α and p85α are shown in the Source data, with peptide exchange data presented in Fig. S6. The changes observed for H1047R matched almost exactly our previous studies[16], but this experiment expanded the HDX time course, allowing for a more in-depth analysis of perturbations in conformation.

The H1047R, G1049R, and the ΔCter constructs showed similar significant increases compared to the WT in the kinase domain (Fig. 5A-C). This included regions

covering 850-858 (hinge between the N and C lobes), the activation loop (930-956), and helices spanning the regulatory arch (1014-1021 in kα10, 1021-1038 in kα11) (Fig. 5A-C). Many of these regions correspond directly to the contact site between the C-terminus and kα11. This validates the inhibitory interaction observed in the 4OVU crystal structure, with this interface stabilising helix kα11 and the activation loop. One region in kα8 (962-980) showed a significant change between H1047R, G1049R and WT, which was not observed comparing WT and ΔCter. This helix contacts both the C-terminus and kα11. A possible mechanism explaining this difference is the rotation that occurs in kα11 upon mutation of H1047R. Structures of free p110α lacking the C-terminus do not show this same rotation of the kα11 helix. The rotation of kα11 would alter the interface between kα8 and kα11, leading to increased exchange in kα8. This could be driven by a unique orientation of the C-terminus packing against kα7 in the H1047R or G1049R mutant, which would be lost in the absence of the C-terminus as would occur in the ΔCter protein. Overall, this data suggests that H1047R and G1049R lead to activation through disruption of the inhibitory conformation of the C-terminal tail, which reorients the lipid binding WIF motif at the membrane binding surface. Both M1043L and N1068fs showed no significant differences compared to WT, suggesting these mutants do not disrupt the inhibitory C-terminal conformation (Fig. 5D+E).

We also compared HDX-MS differences in full-length p110α-p85α between WT, H1047R and ΔC in the presence and absence of pY (Fig. S7). The binding of pY led to significant increases for all three constructs at interfaces that have been previously described (ABD-RBD linker, C2-iSH2, nSH2-helical). However, intriguingly there were unique differences upon pY binding for the ΔCter and H1047R constructs at the interface

of the regulatory arch with the nSH2 domain (1014-1021, kα10). This is intriguing as it suggests that the opening of this portion of the regulatory motif only occurs upon both disengagement of the nSH2 domain (mediated by pY binding) and disengagement of the inhibitory C-terminus (Fig. S7).

Discussion

Understanding how p110α is regulated and how oncogenic *PIK3CA* mutants alter this regulation is essential in the development of novel PI3K therapeutics. Due to the critical homeostatic roles that WT p110α plays in growth, development, and metabolism[41], as well as the cell intrinsic[42,43] and systematic[44] negative feedback loops that oppose PI3K pharmacological inhibition, there are extensive advantages to selectively targeting mutant p110α over WT p110α. Therefore, defining the exact molecular basis underlying mutant specific conformational changes may reveal opportunities for mutant-selective drug design. Oncogenic mutants in p110α span multiple domains of the catalytic subunit, with foci occurring at the ABD, ABD-RBD linker, C2-iSH2 interface, nSH2-helical interface, and the N+C lobes of the kinase domain[35]. While most mis-sense oncogenic mutations discovered in tumours are at hot-spot locations (E542K, E545K, H1047R), more than 25% of all mutations in *PIK3CA* occur outside the hotspots. Extensive biochemical[16] and cellular experiments[45,46] have defined that PIK3CA mutations activate lipid kinase activity by different mechanisms. This together with the recent discovery that multiple mutations in PIK3CA occur *in cis*[33], where hotspot and rare mutations are found in the same gene, highlights the need to fully understand how multiple oncogenic mutations can synergically activate PI3K lipid kinase activity. Here using a suite of

biochemical and biophysical approaches we propose a unifying molecular model for how all *PIK3CA* mutations can lead to increased kinase activity, as well as how different oncogenic mutations *in cis* can increase oncogenicity.

We wanted to define how extensive oncogenic gain of function *PIK3CA* mutations at both the ABD interface and the C2-iSH2 interface activate lipid kinase activity. The critical role of the ABD in regulating p110α kinase activity was originally suggested by its direct interaction with the N-lobe of the kinase domain[15,47]. We previously observed exposure occurring at the ABD interface (ABD-RBD linker) upon phosphopeptide pY binding[16,19], and more extensive exposure at the ABD interface upon membrane binding[12,16]. Cryo EM analysis of p110α with p85α revealed disengagement of the ABD and p85 subunit from the catalytic core of p110α upon binding phosphorylated peptide[27]. To fully define the relative role of ABD disengagement in PI3K activation on membranes we generated the ΔABD p110α catalytic core and directly compared its exchange to the full length p110α-p85α. Increased exposure was seen at all contact interfaces with both p85 and the ABD. Intriguingly, we found that the ΔABD p110α catalytic core showed H/D exchange rates at the ABD-RBD linker that almost exactly matched those observed upon Ras and pY mediated membrane binding of WT p110α-p85α[12]. Importantly, we did not observe similar rates when comparing phosphopeptide bound p110α-p85α, suggesting that complete ABD disengagement only occurred when p110α is membrane bound which is in contrast from what was suggested from the cryo-EM model of PI3Ka in the presence of pY peptides.

We previously observed that mutations at the ABD interface exposed the C2-iSH2 interface, and *vice versa*[16]. As the ABD will always remain tightly bound to the iSH2

domain, its disengagement would likely occur simultaneously with disruption of the C2-iSH2 interface. For these mutants, full disruption of the ABD and C2-iSH2 interfaces occurred only upon removal of the nSH2 (through pY binding), with no requirement for membrane. This reveals an unexpected inhibitory role of the nSH2 domain, whereby packing against the helical, kinase, and C2 domains of p110α and the iSH2 of p85α, it can stabilise the interface with the iSH2 domain, which prevents ABD disengagement from the catalytic core of p110α. Intriguingly, ABD disengagement is likely involved in membrane recruitment for all class IA PI3Ks, as HDX-MS experiments on membranes showed exposure in the iSH2 and the ABD-RBD linker of p110β[48] and p110δ[25,49]. These changes were also seen in primary immunodeficiency mutations of p110δ[50] and in activating *PIK3R1* truncations at the N+C termini of the iSH2 involved in immunodeficiencies and oncogenic transformation[11,49]. An interesting implication in this model is that unique class IA regulatory subunits may have distinctive propensities for ABD-p85 disengagement, which may partially explain a unique role for regulatory subunits oncogenic transformation[51]. This will require further study to investigate regulatory subunit isoform differences in disengagement. Together this highlights the key role of ABD disengagement in PI3K activation, and how oncogenic mutants can alter this regulation.

We next wanted to understand how ABD and p85 disengagement is involved in membrane binding of PI3K. We hypothesized that the free catalytic core of p110α may more efficiently bind to lipid membranes. Our protein-lipid FRET experiments with ΔABD p110α over the pY activated full length p110α-p85α showed enhanced membrane binding similar with our previous studies on the ΔABD construct of p110δ[25]. To

understand the mechanism for how this occurs we mapped the membrane binding interface of ΔABD p110α using HDX-MS. We observed decreased exchange at the C2 and the N-lobe and C-Lobe of the kinase domain. Many of these changes were not observed in the full-length heterodimer upon binding membranes, with these regions located at either the ABD (kα1-kα2 helices of N-lobe) or iSH2 (C2 domain) interfaces. This suggests that some of the membrane binding regions of p110α are shielded by the ABD or p85 subunit, and disengagement of these regions allows for efficient membrane binding. This model also suggests that the role of phosphopeptide binding in membrane recruitment is two-fold as it both breaks an inhibitory contact between the nSH2 and the regulatory motif of the kinase domain, and also breaks the nSH2 contact with the helical domain allowing for disengagement of the ABD and p85 subunits from the catalytic core, exposing membrane binding surfaces of p110α (Fig. 6).

One of the largest decreases in exchange observed upon membrane binding was in the C-terminus of p110α, specifically at the membrane binding WIF motif. In high resolution structures of inhibited p110α, the C-terminus is pointed away from the putative membrane binding surface[37], with the C-terminus pointed towards the membrane surface in the structure of H1047R p110α[17] due to a ~180 rotation at the end of the kα11 helix. The C-terminus in the WT structures makes a set of contacts the regulatory motif helices (kα8- kα11) located after the activation loop, and contacts the C-terminus of the activation loop. The regulatory motif helices and the C-terminus encompass the activation loop and make extensive contacts proposed to maintain an inactive conformation. The regulatory motif is also directly in contact with the nSH2 domain of regulatory subunits. Sequestering the C-terminus in a inhibited conformation is a conserved aspect of regulation across all

class I PI3Ks, with the inhibited conformation of the C-terminus of p110β and p110δ binding to the cSH2 of regulatory subunits[25,52], and p110γ having its C-terminus inhibited by an inhibitory Tryptophan lock which does not require regulatory subunits[32]. Removal of the C-terminus causes a substantial rearrangement of the activation loop, and a rotation of the kα11 helix[53]. Most of the frequent mutations in the C-terminus of p110α would be expected to disrupt this inhibitory contact, either through steric hindrance (M1043I/L, H1047R, G1049R) or disruption of key hydrogen bonds (N1044S). One of the only frequent oncogenic mutations that is not at either the regulatory C-terminus or an interface with the ABD or p85 is located at the loop between kα1-kα2 in the N-lobe (E726K) in a location at the membrane binding surface. This mutant likely drives increased lipid kinase activity through enhanced membrane binding of negatively charged lipids through this charge reversal mutant.

To test if conformational changes in H1047R were caused by disruption of the inhibitory contacts with the C-terminus, we compared the H/D exchange rates of H1047R and a deletion of the C-terminus to the WT protein. The H1047R and C-terminal deletion showed similar increases in exchange in the kα11 helix in contact with the inhibited C-terminus. This suggests a key role of the H1047R mutant is to disrupt inhibitory contacts between the C-terminus and orient the C-terminus in a productive conformation for membrane binding. In addition to this membrane binding role, the removal of the C-terminus also leads to a reorientation of the activation loop, and increased activity towards both ATP hydrolysis and soluble PIP_3 substrate[54]. Therefore, mutations that disrupt this inhibitory C-terminal contact (H1047R, G1049R) activate lipid kinase activity by two unique mechanisms they reorient the WIF motif towards the membrane binding surface,

increasing membrane binding, while also causing the activation loop to adapt a catalytically competent conformation. This explains why we saw increased activity both in solution (ATPase) and on membranes (with PIP_2 sensor).

N1068fs and M1043L caused no significant differences in exchange and ATPase activity, but greatly increased membrane binding, and lipid kinase activity. A putative mechanism explaining this is that the 1068fs replaces the terminal Asn, with a set of positive and hydrophobic residues (KLKR), which all would contribute enhanced membrane binding. So, while the 1068fs mutant does not reorient the membrane binding interface, it likely interacts more extensively, increasing membrane residency time, and increasing PIP_3 production. The M1043L mutant has a much smaller effect on membrane binding. Comparing the structure of WT p110α to H1047R p110α shows a rotation of the kα11 helix in the mutant, with the M1043 residue rotating into where the W1051 from the C-terminus is located in the WT structure[17]. We expect that reorientation of the C-terminus is required for full activity, and therefore we propose that the enhanced membrane binding of M1043L (and potentially M1043I/V) is driven by the added steric bulk of the branched chain amino acids, which may more efficiently reorient the C-terminus upon membrane binding. Further structural studies of the M1043 mutants on membrane surfaces will be required to fully access the molecular basis of activation.

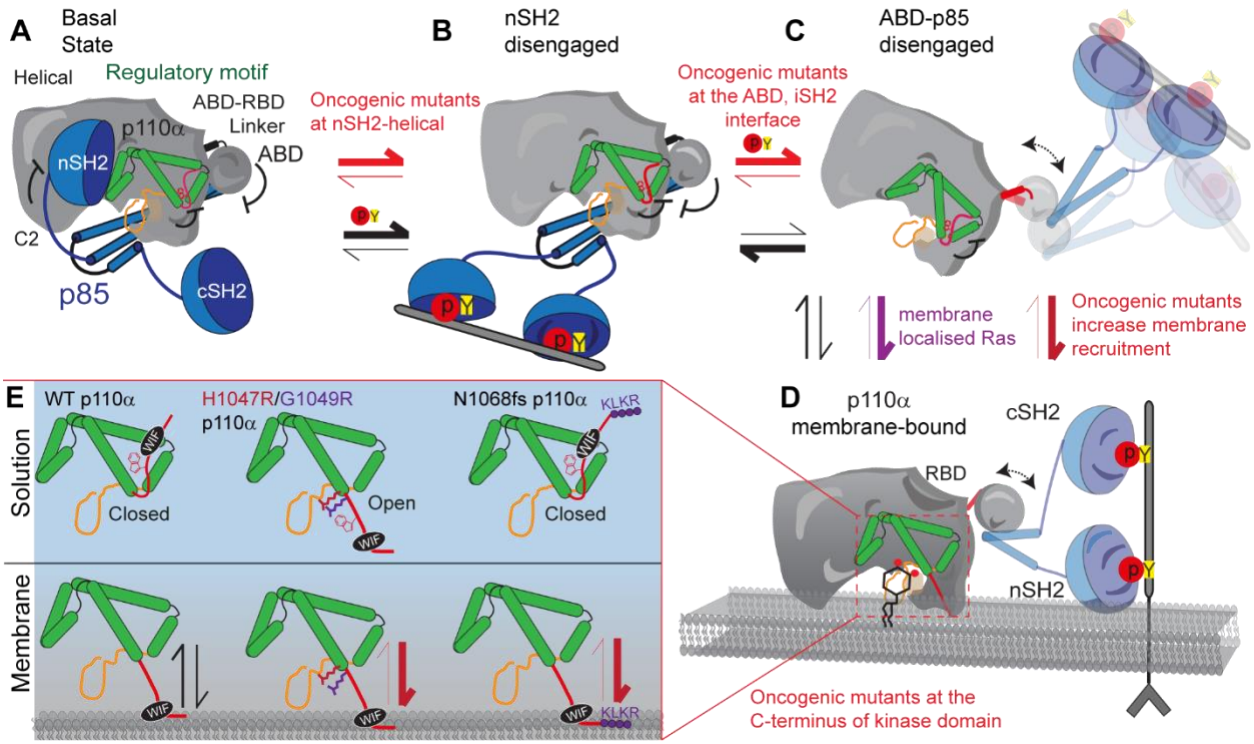

Fig 6. Summary of molecular mechanisms of PI3K inhibition by the ABD and regulatory subunit, and how activation occurs in the wild-type enzyme (black and purple arrows) as well as how oncogenic mutations can alter this process (red arrows).

A cartoon model representing the fully inhibited state is shown in panel **A**, with the nSH2 disengaged state shown in **B** (driven by either pY binding or helical domain mutants), and the ABD-p85 disengaged state shown in **C** (driven by oncogenic mutants at the C2-iSH2 interface and the ABD-interface). The fully active membrane bound state with a reoriented C-terminus is shown in **D**.

E. Different molecular mechanisms driving activation of C-terminal mutations in *PIK3CA*. The regulatory motif is colored green, with the C-terminus colored red, and the activation loop in black (inactive) or red (orange). The C-terminus when in its closed conformation has the membrane binding WIF motif oriented away from the membrane surface. Membrane binding requires the reorientation of this tail, with the membrane itself likely involved in this conformational change. Mutations that disrupt this interface (H1047R, G1049R) are in an open conformation, leading to greatly increased membrane binding. In the N1068fs mutant there is no change in conformation in solution, but the added KLKR motif dramatically increases membrane recruitment.

Overall, integrating our experimental efforts with the extensive previous biophysical and biochemical analysis of p110α mutants we can propose a unifying model for how p110α is inhibited by regulatory subunits, and how it can be activated both by activating partners and oncogenic mutants (Fig. 6). Activation of p110α/p85α by bis-phosphorylated receptors and their adaptors leads to breaking of the inhibitory nSH2 contacts with the p110α subunit. Helical domain mutants (E542K, E545K) mimic this conformational change (red equilibrium arrows between Fig. 6A-6B). The removal of the nSH2 partially destabilises the iSH2-C2 and ABD-kinase interfaces, but in the wild type complex the equilibrium is mainly towards a closed p85-ABD engaged complex (black arrows). The pYXXM binding surface of the nSH2 exposed in helical mutants leads to greatly enhanced recruitment to RTKs and their adaptors[55]. Oncogenic mutations that occur at the ABD or iSH2 interfaces in p110α (red equilibrium arrows between Fig 6B-6C) shifts the equilibrium towards the disengaged state, leading to increased affinity for membranes. Full membrane recruitment still depends on the opening of the C-terminus of p110α. In the wild type complex, membrane recruitment requires additional signalling inputs from Ras GTPases. Oncogenic mutants in the kinase domain lead in increased membrane binding either through reorientation of the WIF binding motif and the activation loop (i.e. H1047R, G1049R), or by altering residues at the membrane interface that can more extensively interact with negatively charged membranes (i.e. E726K, 1068fs) (red equilibrium arrows between Fig. 6C-6D, and 6E). Together, this model can account for the putative mechanism of activation for >98% of all PIK3CA mutants reported in the COSMIC database, and for why double PIK3CA mutants lead to increased oncogenicity (Fig. S8).

Extensive efforts have focused on the development of p110α selective inhibitors. *PIK3CA* mutant selective inhibitors would likely have major advantages in cancer treatment as they can evade feedback mechanisms that counteract pharmacological inhibition of WT *PIK3CA*. Mutant selective inhibitors have been discovered that lead to selective degradation of E545K and H1047R over WT[56], along with recent reports of H1047R selective inhibitors. Our data showing very similar conformational changes in H1047R and G1049R suggest that 1047R/L selective small molecules may also be useful in targeting G1049R/S. There also could be advantages of generating tool compounds that activate PI3K activity, with small molecules that disrupt the ABD or p85 interfaces likely acting as activators. Our findings provide a molecular framework for the future development of the next generation of PI3K modulators as therapeutics.

Acknowledgements

J.E.B. is supported by the Canadian Institute of Health Research (CIHR, 168998), and the Michael Smith Foundation for Health Research (MSFHR, scholar 17686). We also thank the Cho laboratory (University of Illinois Chicago) for providing us with the plasmid for the PIP_2 sensor ENTH domain.

Author Contributions

H.R. and M.R. carried out all biochemical analysis in the manuscript. H.R., M.P., M.L.J., M. R., carried out and analyzed all HDX-MS data. H.R. and J.E.B. designed the experiments and wrote the first draft. All authors contributed to editing.

Conflict of interest statement

J.E.B. reports personal fees from Olema Pharmaceuticals (San Francisco, USA) and Scorpion Therapeutics (Boston, USA).

Data availability statement

The HDX-MS proteomics data generated in this study have been deposited to the ProteomeXchange Consortium via the PRIDE partner repository[58] with the dataset identifier PXD031080. All data generated or analysed during this study are included in the source data excel file.

Materials and Methods

REAGENT or RESOURCE	SOURCE	IDENTIFIER
Bacterial and virus strains		
E.coli XL10-GOLD KanR Ultracompetent Cells	Agilent	200317
E.coli DH10EMBacY Competent Cells	Geneva Biotech	DH10EMBacY
Chemicals, peptides, and recombinant proteins		
H2N-ESDGG(pY)MDMSKDESID(pY)VPMLDMKGDIKYADIE-OH	New England Peptide	N/A
Deuterium Oxide 99.9%	Sigma Aldrich	151882-10X1ML
ATP	Sigma	A7699- 1g
sodium deoxycholate	Sigma	D6750
Protease inhibitor cocktail	Sigma	535140
Polyoxyethylene (10) lauryl ether	Sigma	P9769
Phosphatidylserine (Porcine Brain)	Avanti	840032C
Phosphatidylethanolamine (Egg yolk)	Sigma Aldrich	P6386
Cholesterol	Sigma Aldrich	47127-U
Phosphatidylcholine (Egg yolk)	Avanti	840051C
Phosphatidylinositol-4,5-bisphosphate (Porcine Brain)	Avanti	840046
Sphingomyelin (Egg yolk)	Sigma Aldrich	S0756
Dansyl-Phosphatidyl Serine	Avanti	810225C
6-well sticky-side chamber	IBIDI	80608
Polyethanolamine (PEI)	Polysciences	24765
Critical commercial assays		
Transcreener ADP2 FI Assay (1,000 Assay, 384 Well)	BellBrook Labs	3013-1K
Oligonucleotides		
Forward Primer for D915∗ mutation in p110α-CCTTCATTTTGGGAATTGGAaatCGTCACAATAGTAACATCATGGTGAAAGACG	Sigma Aldrich	oHP006F

Reverse Primer for D915∗ mutation in p110α-attTCCAATTCCCAAAATGAAGGTAGCTACACAG	Sigma Aldrich	oHP006R
Forward Primer for H1047R∗ mutation in p110α-CAAATGAATGATGCACgTCATGGTGGCTGGACAACAAAAATGG	Sigma Aldrich	MR81f
Reverse Primer for H1047R mutation in p110α-TGCATCATTCATTTGTTTCATGAAATACTCCAAAGC	Sigma Aldrich	MR81R
Forward Primer for M1043L mutation in p110α-GAGTATTTCATGAAACAAcTGAATGATGCACATCATGGTGGCTGG	Sigma Aldrich	MR82F
Reverse Primer for M1043L mutation in p110α-TTGTTTCATGAAATACTCCAAAGCCTCTTGC	Sigma Aldrich	MR82R
Forward Primer for G1049R∗ mutation in p110α-ATGATGCACATCATcGTGGCTGGAC	Sigma Aldrich	oHP005F
Reverse Primer for G1049R mutation in p110α-ACgATGATGTGCATCATTCATTTGTTTCATGAAATACTC	Sigma Aldrich	oHP005R
Forward Primer for N1068KLKR mutation in p110α-ATGCATTGAAACTTAAAAGGTGAgcggccgctcgagtctag	Sigma Aldrich	oHP004F
Reverse Primer for N1068KLKR mutation in p110α-CCTTTTAAGTTTCAATGCATGCTGTTTAATTGTGTGGAAGATC	Sigma Aldrich	oHP004R
Forward Primer for ∆C mutation in p110α-GGCgccggtaccATGCCTCCACGACCATCATCAGG	Sigma Aldrich	MR80F
Reverse Primer for ∆C mutation in p110α-agcggccgcTCAATGATGTGCATCATTCATTTGTTTCATGAAATAC	Sigma Aldrich	MR86R
Forward Primer for ∆ABD mutation in p110α-GGGCgccggtaccAACCGTGAAGAAAAGATCCTCAATCGAG	Sigma Aldrich	oHP008F
Reverse Primer for ∆ABD mutation in p110α-GGATCTTTTCTTCACGGTTggtaccggcGCCCTGAAAATAC	Sigma Aldrich	oHP008R
Recombinant DNA		
Human p110α (1-1068)	Dornan G L et al., 2020[11]	GD102
p110α H1047R	This paper	MR98
p110α M1043L	This paper	MR100
p110α G1049R	This paper	HP15
p110α with N1068KLKR	This paper	HP14
p110α ∆Cter (1-1048)	This paper	MR106
p110α ∆ABD (106-1068)	This paper	HP31
Human p85α (1-724)	Dornan G L et al., 2020[11]	EX20
p110α D915N (1-1068)	This paper	HP16
p110α D915N and H1047R	This paper	HP19
p110α D915 and M1043L	This paper	HP25
p110α D915 and G1049R	This paper	HP27
p110α D915 and N1068KLKR	This paper	HP26
ENTH domain	Sun J et al., 2020[40]	HP33
Software and algorithms		

HDExaminer	Sierra Analytics	http://massspec.com/hdexaminer
GraphPad Prism 7	GraphPad	https://www.graphpad.com
Adobe Illustrator	Adobe	https://www.adobe.com/products/illustrator.html
COSMIC: Catalogue Of Somatic Mutations In Cancer	Sanger;	https://cancer.sanger.ac.uk/cosmic
PyMOL	Schroedinger	http://pymol.org
Other		
Sf9 insect cells for expression	Expression Systems	94-001S

Plasmid Generation

Plasmids harbouring WT p110α and p85α were previously described but in short, genes of interest were inserted into the pFastBac1 vector to allow baculovirus expression in *Spodoptera frugiperda* (Sf9) cells. The plasmids containing p110 isoforms also expressed N-terminal to the protein a 10X histidine tag, followed by a 2X Strep tag, followed by a Tobacco Etch Virus protease cleavage site. Single substitution mutations (D915N, H1047R, M1043L, G1049R and N1068fs) and p110 truncations (ΔABD and ΔC) were generated using site-directed mutagenesis according to published commercial protocols (QuickChange Site-Directed Mutagenesis, Novagen). DNA oligonucleotides spanning the desired region and either containing the altered nucleotides (single substitutions) or lacking the truncated region were ordered (Sigma). PCR reactions were performed on the WT p85α, and PCR purified (Q5 High-Fidelity 2X MasterMix, New England Biosciences #M0492L; QiaQuick PCR Purification Kit, Qiagen #28104). Single colonies were grown overnight and purified using QIAprep Spin Miniprep Kit (Qiagen #27104). Plasmid identity was confirmed by sanger sequencing (Eurofins Genomics).

Virus Generation and Amplification

The pFastBac plasmids harbouring p110α WT and other variants and p85α were transformed into DH10MultiBac cells (MultiBac, Geneva Biotech) containing the MultiBac baculovirus viral genome (bacmid) and a helper plasmid expressing transposase to transpose the expression cassette harbouring the gene of interest into the baculovirus genome. Bacmids with successful incorporation of the expression cassette of pFastBac into the MultiBac viral genome were identified by blue-white screening and were purified from a single white colony using a standard isopropanol-ethanol extraction method. Briefly, colonies were grown overnight (~16 hours) in 3-5 mL 2xYT (BioBasic #SD7019). Cells were pelleted by centrifugation and the pellet was resuspended in 225 µL P1 Buffer (Qiagen MiniPrep Kit, #27106), chemically lysed by the addition of 225 µL Buffer P2, and the lysis reaction was neutralized by addition of 300 µL Buffer N3. Following centrifugation at 21130 rcf and 4°C (Rotor #5424 R), the supernatant was separated and mixed with 600 µL isopropanol to precipitate the DNA out of solution. Further centrifugation at the same temperature and speed pelleted the Bacmid DNA, which was then washed with 500 µL 70% Ethanol three times. The Bacmid DNA pellet was then dried for 1 minute and re-suspended in 50 µL Buffer EB.

Purified bacmid was then transfected into Sf9 cells. 2 mL of Sf9 cells between 0.3-0.5X10^6 cells/mL were aliquoted into the wells of a 6-well plate and allowed to attach, creating a monolayer of cells at ~ 70-80% confluency. Transfection reactions were prepared by the addition of 2-10 ug of bacmid DNA to 100 µl 1xPBS and 12 µL polyethyleneimine (PEI) at 1 mg/mL (Polyethyleneimine “Max” MW 40.000, Polysciences #24765, USA) to 100 µL 1xPBS. The bacmid-PBS and the PEI-PBS solutions were mixed, and the reaction occurred for 20-30 minutes before addition drop-by-drop to an

Sf9 monolayer containing well. Transfections were allowed to proceed for 5-7 days before harvesting virus containing supernatant as a PI viral stock.

Viral stocks were amplified by adding P1 viral stock to suspension Sf9 cells between 1-2x106 cells/mL at a 1/100 volume ratio. This amplification produces a P2 stage viral stock that can be used in final protein expression. The amplification proceeded for 4-5 days before harvesting, with cell shaking at 120 RPM in a 27°C shaker (New Brunswick). Harvesting of P2 viral stocks was carried out by centrifuging cell suspensions in 50 mL Falcon tubes at 2281 RCF (Beckman GS-15), collecting the supernatant in a fresh sterile tube, and adding 5-10% inactivated foetal bovine serum (FBS; VWR Canada #97068-085).

Expression and purification of recombinant proteins

All PI3K constructs were purified by expressing the catalytic subunit and the regulatory subunit using bacµLovirus MultiBac expression system in SF9 cells. After expressing the cells at 27 °C (42 hours for Kinase active variants and 55 hours for Kinase dead), the cells were harvested at 2800 rpm and 4C using Eppendorf Centrifuge 5810R and the cells were flash frozen using liquid nitrogen and stored in -80C. The proteins were purified by a series of affinity chromatography techniques that includes Nickel affinity, Streptavidin and Q column.

The frozen pellets were resuspended in lysis buffer containing 20 mM Tris pH 8, 10 mM Imidazole, 100 mM NaCl, 5% glycerol [v/v], 2 mM βME, protease inhibitor [Protease Inhibitor Cocktail Set III, Sigma]) and sonicated for 2 min (15 s on, 15 s off, level 4.0, Misonix sonicator 3000). Triton-X was added to the lysate at a final

concentration of 0.1% and then clarified by spinning at 14, 000 rpm for 45 min (Beckman Coulter JA-20 rotor). The supernatant was loaded onto a 5 ml crude Ni-NTA column (GE healthcare) equilibrated in NiNTA A buffer containing 20 mM Tris pH 8, 100 mM NaCl, 10 mM Imidazole and 5% glycerol [v/v]. The column was washed using high salt buffer containing 20 mM Tris, 1 M NaCl, 10 mM Imidazole, 5% Glycerol [v/v] followed by NiNTA buffer wash (20 mM Tris pH 8, 100 mM NaCl, 21 mM Imidazole and 5% Glycerol). The protein was eluted using 100% NiNTA B buffer (20 mM Tris pH 8, 100 mM NaCl, 200 mM Imidazole and 5% Glycerol). The elute from the nickel column was loaded onto Streptavidin column (GE healthcare) and subjected to buffer wash using Hep A buffer (20 mM Tris pH 8, 100 mM NaCl, 5% Glycerol and 0.5 mM tris(2-carboxyethyl) phosphine [TCEP]). The column was incubated on ice for 3 hours in the presence of TEV protease and then eluted by a wash with HEP A buffer. The eluent was loaded onto Q column equilibrated with HEP A buffer. The column was washed with HEP A buffer to remove TEV protease and the final PI3K was eluted by passing Hep B elution buffer (20 mM Tris pH 8, 325mM NaCl, 5% glycerol [v/v] and 0.5 mM TCEP). The protein was exchanged to the final buffer containing 20 mM HEPES pH 7.5, 100 mM NaCl, 10 % Glycerol [v/v] and 0.5 mM TCEP using a desalting column. The protein was concentrated to 1 mg/ml using a 50,000 MWCO Amicon Concentrator (Millipore), flash frozen and stored at -80°C.

For HDX experiments involving WT, ΔABD, H1047R, M1043L and ΔCter were further subjected to gel filtration using Superdex^{TM} 200 10/300 GL Increase from GE healthcare. After gel filtration, the protein was concentrated, aliquoted, frozen, and stored at −80°C.

For direct measurement of PIP_2, we purified the modified sensor consisting of Epsin 1 NTerminal Homology (ENTH) domain by expressing the protein in C41 (DE3) E. coli cells. Protein expression was induced overnight at room temperature with 0.5 mM (final concentration) isopropyl β-d-1-thiogalactopyranoside when the optical density of the media reached 0.6-0.8. The frozen pellets were resuspended in lysis buffer containing 20 mM Tris pH 8, 50 mM NaCl, 5% Glycerol and 0.5 mM tris(2-carboxyethyl) phosphine [TCEP], protease inhibitor [Protease Inhibitor Cocktail Set III, Sigma]) and sonicated for 5 min (15s on, 15s off, level 6.0, Misonix sonicator 3000). Triton-X was added to the lysate at a final concentration of 0.1% and the clarified by spinning at 14, 000 rpm for 45 min (Beckman CoµLter JA-20 rotor). The supernatant was loaded onto a 5 ml GST column (GE healthcare) equilibrated in HEP A buffer containing 20 mM Tris pH 8, 50 mM NaCl, 5% Glycerol and 0.5 mM tris(2-carboxyethyl) phosphine [TCEP] followed by 2 column volume buffer wash with labelling buffer (50 mM Tris-HCl, 300 mM NaCl, 1 mM TCEP, 50 mM arginine, 50 mM glutamic acid (pH 8.0). The column was incubated overnight at 4°C in the presence of thrombin protease (Sigma, T4648). The cleaved protein was eluted with gel filtration buffer consisting of (50 mM Tris-HCl, 300 mM NaCl, 1 mM TCEP, 50 mM arginine, 50 mM glutamic acid (pH 8.0)). This was incubated with 3-fold excess fluorophore ‘acrylodan’ (6-Acryloyl-2-Dimethylaminonaphthalene) from Invitrogen (A4333) at room temperature for two hours. This was then concentrated using a 10,000 MWCO Amicon Concentrator (Millipore) and subjected to gel filtration using Superdex™ 75 10/300 GL Increase from GE healthcare. After gel filtration, the protein was concentrated, aliquoted, frozen, and stored at −80°C.

Lipid Vesicle Preparation

For lipid kinase assay measuring the activities of PI3K mutants, PIP_2/PS/PE membranes were made by mixing 5 % brain Phosphotidylinositol 4, 5 Bisphosphate (PIP_2) (Avanti, #840046), 65% egg yolk Phosphotidylethanolamine (PE) and 35 % brain Phosphotidylseine (PS) (Avanti, #840032C). To measure membrane recruitment using Protein-Lipid FRET two sets of lipid vesicles were prepared: PE/PS/PIP_2 containing 5 % brain PIP_2, 65% egg yolk PE, 25 % brain PS and 10% Dansyl-PS (Avanti, #810225C) and PM mimic consisting of 5% brain PIP_2, 20% brain PS, 10% Dansyl-PS, 45% egg yolk PE, 15% egg yolk phosphatidylcholine (PC) (Avanti #840051C), 10% cholesterol (Sigma Aldrich, #47127-U), and 5% egg yolk sphingomyelin (Sigma Aldrich, #S0756). To generate vesicles the lipid mixtures were combined in organic solvent. The mixture was then evaporated using a stream of argon gas followed by desiccation under vacuum for 45 minutes. The lipids were resuspended in a lipid buffer (25 mM HEPES pH 7, 100 mM NaCl, 10% Glycerol [v/v] and the solution was subjected to sonication for 15 mins. The vesicles were subjected to five freeze thaw cycles and extruded 11 times through a 100 nm filter (T and T Scientific: TT-002–0010). The extruded vesicles were sonicated again for 5 min, aliquoted and stored at −80°C.

Protein-Lipid FRET Assay

Protein-lipid FRET experiments were carried out either at a saturating protein concentration (Fig. 4F) or as a dose response with PI3K (Fig. S4G). Protein lipid FRET assays with saturating PI3K were initiated by mixing 2.5 µL PI3K (4 µM) with 2.5 µL of pY peptide (final conc) for 15 mins at 20°C. 5 µL of lipid vesicles (either PIP_2/PS/PE or PM

mimic vesicles, both at final conc. 33.33 µg/mL) was added to the protein-pY mixture and were incubated for 15 mins at 20°C. Dose experiment was carried out exactly the same, except PI3K amount varied from 0.015 µM to 1 µM. The plate was then read using a SpectraMax M5 plate reader using a 280-nm excitation filter with 350-nm and 520- nm emission filters to measure Trp and Dansyl-PS FRET emissions, respectively. The FRET signal shown in the figure has $I-I_o$ along the Y axis where I is the intensity of 520 with protein and Io is the intensity of lipid alone. for dose response curve (Fig. S3)

Lipid kinase assays

Lipid kinase assays were done using a slightly modified procedure from[40]. The kinase buffer contains 20 mM HEPES pH 7.5, 100 mM NaCl, 7 mM MgCl2, 50 µM CHAPS and 2 mM TCEP and the quench buffer contains 20 mM HEPES pH 7.5 and 40 mM EDTA. For assays measuring the kinase activities of WT and mutants, a final of 1 mg/ml of PIP_2/PS/PE vesicles was used and 1 µM pY peptide. 1.5 µL of protein 4X final concentration was mixed with 1.5 µL of pY peptide and allowed to incubate at 20°C for 10 minutes to allow pY activation. The reaction was started by adding 3µL of 2X vesicles with 1µM ATP and the reaction was allowed to proceed for 60 minutes at 37°C. The reaction was then quenched by adding 3 µL of quench buffer and 0.5 µM of the ENTH PIP_2 sensor. The fluorescence intensity was measured using a SpectraMax M5 plate reader at excitation 380 nm where the sensor displays a blue shift in fluorescence emission peak from 530 to 470 nm upon membrane binding (caused by changes in hydrophobicity and exposure to solvent) and the intensity at 470 nm is increased proportionally to the concentration of the PIP_2. The data was plotted with concentration

along x-axis and F_{470}/F_{530} along Y-axis. The data was normalized using no kinase lipid condition as maxima and highest protein-pY concentration condition as minima.

ATPase assay

All ATPase assays employed Transcreener ADP2 Fluorescence Intensity (FI) Assay (Bellbrook labs) which measures ADP production. For the assays measuring the ATPase activity Two µL of a kinase solution at 2X final concentration was mixed with 2 µL substrate solution containing ATP and the reaction was allowed to proceed for 60 min at 20°C. The reaction was stopped with 4 µL of 2X stop and detect solution containing Stop and Detect buffer along with 8 nM ADP Alexa Fluor 594 Tracer and 93.7 µg/mL ADP2 Antibody IRDye QC-1 and incubated for 50 min. The fluorescence intensity was measured using a SpectraMax M5 plate reader at excitation 590 nm and emission 620 nm. This data was normalised against a 0–100% ADP window made using conditions containing either 100 µM ATP/ADP with vesicles and kinase buffer. % ATP turnover was interpolated from an ATP standard curve obtained from performing the assay on 100 µM (total) ATP/ADP mixtures with increasing concentrations of ADP.

HDX-MS analysis: ***Sample Preparation***

HDX-MS experiments for all conditions were conducted as follows: reactions comparing full-length p110α/p85α and ΔABD p110α were conducted in 13.5-µl reaction volumes with a final PI3K amount of 10 pmol. Prior to HD exchange, 3.5 µl of either protein was incubated with 3.5 µl of PIP_2/PS/PE lipid at 1 mg/ml or lipid buffer for 2 minutes at room temperature. To initiate HD exchange, a mixture of either 6.5 µl of the same lipid at

785 1 mg/ml or lipid buffer and 36.5 µl of D_2O buffer [20 mM HEPES (pH 7.5), 100 mM NaCl,
786 94.3% D_2O (v/v)] was added to the protein-lipid/buffer mix (final D_2O concentration of
787 69%). Exchange was carried out for 3, 30, and 300s at 20°C.

788 HDX reactions comparing full-length p110α/p85α WT against M1043L, H1047R
789 and ΔC were conducted in 20µl reaction volumes with a final PI3K amount of 9 pmol. Prior
790 to HD exchange, 3 µl of protein was incubated with 1µl of 50 µM pY peptide or protein
791 buffer and allowed to incubate for 15 minutes on ice. Exchange was initiated by the
792 addition of 16 µl of D_2O buffer to the protein +/- pY mixture (final D_2O concentration of
793 75%). Exchange was carried out for 3, 30, 300, and 3000s at 20°C and 0.3s (3s on ice).

794 HDX reactions comparing full-length p110α/p85α WT against G1049R were
795 conducted in 20µl reaction volumes with a final PI3K amount of 15 pmol. HD exchange
796 was initiated by the addition of 16 µl of D_2O buffer to 4 µl of protein (final D_2O
797 concentration of 70%). The reaction proceeded for 3, 30, 300, and 3000s at 20°C.

798 HDX reactions comparing full-length p110α/p85α WT against N1068fs were
799 conducted in 20µl reaction volumes with a final PI3K amount of 11 pmol. HD exchange
800 was initiated by the addition of 17.2 µl of D_2O buffer to 2.8 µl of protein (final D_2O
801 concentration of 81%). The reaction proceeded for 3, 30, 300, and 3000s at 20°C.

802 HDX reactions comparing full-length p110α/p85α WT kinase active vs kinase dead
803 were conducted in 50 µl reaction volumes with a final PI3K amount of 10 pmol. Prior to
804 HD exchange, 4 µl of either protein was incubated with 10 µl of PIP_2/PS/PE lipid at 1
805 mg/ml or lipid buffer for 2 minutes at 20°C. HD exchange was initiated by the addition of
806 36 µl of D_2O buffer (final D_2O concentration of 69%). The reaction proceeded for 3, 30,
807 and 300s at 20°C. All conditions and timepoints were generated in independent triplicate.

All exchange reactions were terminated by the addition of ice-cold quench buffer to give a final concentration 0.6 M guanidine-HCl and 0.9% formic acid. Samples were flash frozen in liquid nitrogen immediately after quenching and stored at −80°C until injected onto the ultra-performance liquid chromatography (UPLC) system for proteolytic cleavage, peptide separation, and injection onto a QTOF for mass analysis, described below.

HDX-MS analysis: ***Protein digestion and tandem MS data collection***

Protein samples were rapidly thawed and injected onto an integrated fluidics system containing an HDx-3 PAL liquid handling robot and climate-controlled (2°C) chromatography system (LEAP Technologies), a Dionex Ultimate 3000 UHPLC system, and an Impact HD QTOF mass spectrometer (Bruker). The protein was run over one immobilized pepsin column (Trajan; ProDx protease column, 2.1 mm x 30 mm PDX.PP01-F32) at 200 µl/min for 3 min at 10°C. The resulting peptides were collected and desalted on a C18 trap column [Acquity UPLC BEH C18 1.7 mm column (2.1 x 5 mm); Waters 186003975]. The trap was subsequently eluted in line with an ACQUITY 1.7 µm particle, 100 x 1 mm^2 C18 UPLC column (Waters 186002352), using a gradient of 3-35% B (buffer A, 0.1% formic acid; buffer B, 100% acetonitrile) over 11 min immediately followed by a gradient of 35-80% B over 5 minutes. MS experiments acquired over a mass range from 150 to 2200 mass/charge ratio (m/z) using an electrospray ionization source operated at a temperature of 200°C and a spray voltage of 4.5 kV.

HDX-MS analysis: ***Peptide identification***

Peptides were identified from the nondeuterated samples of p110α/p85α complex for WT and other mutants using data-dependent acquisition following tandem MS

(MS/MS) experiments (0.5-s precursor scan from 150 to 2000 m/z: 12 0.25s fragment scans from 150 to 2000 m/z). MS/MS datasets were analyzed using PEAKS7 (PEAKS), and peptide identification was carried out by using a false discovery–based approach, with a threshold set to 1% using a database of purified proteins and known contaminants found in SF9 cells[57]. The search parameters were set with a precursor tolerance of 20 parts per million, fragment mass error 0.02 Da, and charge states from 1 to 8.

HDX-MS analysis: ***Mass analysis of peptide centroids and measurement of deuterium incorporation***

HD-Examiner Software (Sierra Analytics) was used to automatically calculate the level of deuterium incorporation into each peptide. All peptides were manually inspected for correct charge state, correct retention time, and appropriate selection of isotopic distribution. Deuteration levels were calculated using the centroid of the experimental isotope clusters. HDX-MS results are presented with no correction for back exchange shown in the Source data, with the only correction being applied correcting for the deuterium oxide percentage of the buffer used in the exchange (69% for ΔABD experiments, 69% for WT vs M1043L, H1047R and ΔC, 70% for WT vs G1049R, 81% for WT vs N1068fs and 69% for WT kinase active vs kinase dead). Attempts to generate a fully deuterated class I PI3K sample were unsuccessful, which is common for large macromolecular complexes. Therefore, all deuterium exchange values are relative.

Differences in exchange in a peptide were considered significant if they met all three of the following criteria: ≥5% change in exchange, ≥0.4 Da difference in exchange, and a P-value of <0.01 using a two-tailed Student's t test. The raw HDX data are shown in two different formats.

The raw data for all analysed peptides is available in the source data. The differences in deuterium exchange are visualised in different ways. To allow for visualization of differences across conditions, we used number of deuteron difference (#D) plots (Figs. 2C, 3D, 5A-E, S3C-E, S4A+C, S6A, S7D-F). These plots show the total difference in deuterium incorporation over the entire HDX time course, with each point indicating a single peptide. These graphs are calculated by summing the differences at every time point for each peptide and propagating the error. For a selection of peptides, we are showing the %D incorporation over a time course, which allows for comparison of multiple conditions at the same time for a given region (Figs. 2D+3E, S3F, S4B+D, S6B+C, S7G). Samples were only compared when they were set at the same time and were never compared to experiments completed with a different final D_2O level. The data analysis statistics for all HDX-MS experiments are in table S1 according to published guidelines. The HDX-MS proteomics data generated in this study have been deposited to the ProteomeXchange Consortium via the PRIDE partner repository[58] with the dataset identifier PXD031080.

References

1. Samuels, Y. *et al.* High frequency of mutations of the PIK3CA gene in human cancers. *Science* **304**, 554 (2004).
2. Lawrence, M. S. *et al.* Discovery and saturation analysis of cancer genes across 21 tumour types. *Nature* **505**, 495–501 (2014).
3. Bailey, M. H. *et al.* Comprehensive Characterization of Cancer Driver Genes and Mutations. *Cell* **173**, 371-385.e18 (2018).
4. Goncalves, M. D., Hopkins, B. D. & Cantley, L. C. Phosphatidylinositol 3-Kinase, Growth Disorders, and Cancer. *N Engl J Med* **379**, 2052–2062 (2018).
5. Burke, J. E. Structural Basis for Regulation of Phosphoinositide Kinases and Their Involvement in Human Disease. *Mol. Cell* **71**, 653–673 (2018).
6. Burke, J. E. & Williams, R. L. Synergy in activating class I PI3Ks. *Trends in Biochemical Sciences* **40**, 88–100 (2015).
7. Madsen, R. R. & Vanhaesebroeck, B. Cracking the context-specific PI3K signaling code. *Sci Signal* **13**, eaay2940 (2020).

8. Yu, J. *et al.* Regulation of the p85/p110 phosphatidylinositol 3'-kinase: stabilization and inhibition of the p110alpha catalytic subunit by the p85 regulatory subunit. *Mol. Cell. Biol.* **18**, 1379–1387 (1998).
9. Yu, J., Wjasow, C. & Backer, J. M. Regulation of the p85/p110alpha phosphatidylinositol 3'-kinase. Distinct roles for the n-terminal and c-terminal SH2 domains. *J Biol Chem* **273**, 30199–30203 (1998).
10. Carpenter, C. L. *et al.* Phosphoinositide 3-kinase is activated by phosphopeptides that bind to the SH2 domains of the 85-kDa subunit. *J Biol Chem* **268**, 9478–9483 (1993).
11. Dornan, G. L. *et al.* Defining How Oncogenic and Developmental Mutations of PIK3R1 Alter the Regulation of Class IA Phosphoinositide 3-Kinases. *Structure* **28**, 145-156.e5 (2020).
12. Siempelkamp, B. D., Rathinaswamy, M. K., Jenkins, M. L. & Burke, J. E. Molecular mechanism of activation of class IA phosphoinositide 3-kinases (PI3Ks) by membrane-localized HRas. *J. Biol. Chem.* **292**, 12256–12266 (2017).
13. Buckles, T. C., Ziemba, B. P., Masson, G. R., Williams, R. L. & Falke, J. J. Single-Molecule Study Reveals How Receptor and Ras Synergistically Activate PI3Kα and PIP3 Signaling. *Biophys. J.* **113**, 2396–2405 (2017).
14. Huang, C.-H. *et al.* The structure of a human p110alpha/p85alpha complex elucidates the effects of oncogenic PI3Kalpha mutations. *Science* **318**, 1744–1748 (2007).
15. Miled, N. *et al.* Mechanism of two classes of cancer mutations in the phosphoinositide 3-kinase catalytic subunit. *Science* **317**, 239–242 (2007).
16. Burke, J. E., Perisic, O., Masson, G. R., Vadas, O. & Williams, R. L. Oncogenic mutations mimic and enhance dynamic events in the natural activation of phosphoinositide 3-kinase p110α (PIK3CA). *Proc. Natl. Acad. Sci. U.S.A.* **109**, 15259–15264 (2012).
17. Mandelker, D. *et al.* A frequent kinase domain mutation that changes the interaction between PI3Kalpha and the membrane. *Proc. Natl. Acad. Sci. U.S.A.* **106**, 16996–17001 (2009).
18. Chakrabarti, M., Gabelli, S. B. & Amzel, L. M. Allosteric Activation of PI3Kα Results in Dynamic Access to Catalytically Competent Conformations. *Structure* **28**, 465-474.e5 (2020).
19. Burke, J. E. & Williams, R. L. Dynamic steps in receptor tyrosine kinase mediated activation of class IA phosphoinositide 3-kinases (PI3K) captured by H/D exchange (HDX-MS). *Adv Biol Regul* **53**, 97–110 (2013).
20. Gkeka, P. *et al.* Investigating the structure and dynamics of the PIK3CA wild-type and H1047R oncogenic mutant. *PLoS Comput. Biol.* **10**, e1003895 (2014).
21. Walker, E. H., Perisic, O., Ried, C., Stephens, L. & Williams, R. L. Structural insights into phosphoinositide 3-kinase catalysis and signalling. *Nature* **402**, 313–320 (1999).
22. Rostislavleva, K. *et al.* Structure and flexibility of the endosomal Vps34 complex reveals the basis of its function on membranes. *Science* **350**, aac7365 (2015).
23. Rathinaswamy, M. K. *et al.* Structure of the phosphoinositide 3-kinase (PI3K) p110γ-p101 complex reveals molecular mechanism of GPCR activation. *Sci Adv* **7**, eabj4282 (2021).

24. Wu, H. *et al.* Regulation of Class IA PI 3-kinases: C2 domain-iSH2 domain contacts inhibit p85/p110alpha and are disrupted in oncogenic p85 mutants. *Proc. Natl. Acad. Sci. U.S.A.* **106**, 20258–20263 (2009).
25. Burke, J. E. *et al.* Dynamics of the phosphoinositide 3-kinase p110δ interaction with p85α and membranes reveals aspects of regulation distinct from p110α. *Structure* **19**, 1127–1137 (2011).
26. Zhang, X. *et al.* Structure of lipid kinase p110β/p85β elucidates an unusual SH2-domain-mediated inhibitory mechanism. *Mol Cell* **41**, 567–578 (2011).
27. Liu, X. *et al.* Cryo-EM structures of PI3Kα reveal conformational changes during inhibition and activation. *Proc Natl Acad Sci U S A* **118**, e2109327118 (2021).
28. Jaiswal, B. S. *et al.* Somatic Mutations in p85α Promote Tumorigenesis through Class IA PI3K Activation. *Cancer Cell* **16**, 463–474 (2009).
29. Dornan, G. L. & Burke, J. E. Molecular Mechanisms of Human Disease Mediated by Oncogenic and Primary Immunodeficiency Mutations in Class IA Phosphoinositide 3-Kinases. *Front Immunol* **9**, 575 (2018).
30. Spangle, J. M. *et al.* PIK3CA C-terminal frameshift mutations are novel oncogenic events that sensitize tumors to PI3K-α inhibition. *Proc Natl Acad Sci U S A* **117**, 24427–24433 (2020).
31. Sun, M., Hillmann, P., Hofmann, B. T., Hart, J. R. & Vogt, P. K. Cancer-derived mutations in the regulatory subunit p85 of phosphoinositide 3-kinase function through the catalytic subunit p110. *Proceedings of the National Academy of Sciences* **107**, 15547–15552 (2010).
32. Rathinaswamy, M. K. *et al.* Disease-related mutations in PI3Kγ disrupt regulatory C-terminal dynamics and reveal a path to selective inhibitors. *Elife* **10**, e64691 (2021).
33. Vasan, N. *et al.* Double PIK3CA mutations in cis increase oncogenicity and sensitivity to PI3Kα inhibitors. *Science* **366**, 714–723 (2019).
34. Miller, M. S. *et al.* Structural basis of nSH2 regulation and lipid binding in PI3Kα. *Oncotarget* **5**, 5198–5208 (2014).
35. Tate, J. G. *et al.* COSMIC: the Catalogue Of Somatic Mutations In Cancer. *Nucleic Acids Res.* **47**, D941–D947 (2019).
36. Hon, W. C., Berndt, A. & Williams, R. L. Regulation of lipid binding underlies the activation mechanism of class IA PI3-kinases. *Oncogene* **31**, 3655–3666 (2012).
37. Furet, P. *et al.* Discovery of NVP-BYL719 a potent and selective phosphatidylinositol-3 kinase alpha inhibitor selected for clinical evaluation. *Bioorganic & Medicinal Chemistry Letters* **23**, 3741–3748 (2013).
38. Barsanti, P. A. *et al.* Structure-Based Drug Design of Novel Potent and Selective Tetrahydropyrazolo[1,5-a]pyrazines as ATR Inhibitors. *ACS Med Chem Lett* **6**, 37–41 (2015).
39. Han, W. *et al.* Discovery of imidazo[1,2-a]-pyridine inhibitors of pan-PI3 kinases that are efficacious in a mouse xenograft model. *Bioorg Med Chem Lett* **26**, 742–746 (2016).
40. Sun, J., Singaram, I., Soflaee, M. H. & Cho, W. A direct fluorometric activity assay for lipid kinases and phosphatases. *J Lipid Res* **61**, 945–952 (2020).
41. Fruman, D. A. *et al.* The PI3K Pathway in Human Disease. *Cell* **170**, 605–635 (2017).

42. Sun, S.-Y. *et al.* Activation of Akt and eIF4E survival pathways by rapamycin-mediated mammalian target of rapamycin inhibition. *Cancer Res* **65**, 7052–7058 (2005).
43. Chakrabarty, A., Sánchez, V., Kuba, M. G., Rinehart, C. & Arteaga, C. L. Feedback upregulation of HER3 (ErbB3) expression and activity attenuates antitumor effect of PI3K inhibitors. *Proc Natl Acad Sci U S A* **109**, 2718–2723 (2012).
44. Hopkins, B. D. *et al.* Suppression of insulin feedback enhances the efficacy of PI3K inhibitors. *Nature* **560**, 499–503 (2018).
45. Zhao, L. & Vogt, P. Helical domain and kinase domain mutations in p110alpha of phosphatidylinositol 3-kinase induce gain of function by different mechanisms. *Proc. Natl. Acad. Sci. U.S.A.* **105**, 2652–2657 (2008).
46. Gymnopoulos, M., Elsliger, M.-A. & Vogt, P. K. Rare cancer-specific mutations in PIK3CA show gain of function. *Proc. Natl. Acad. Sci. U.S.A.* **104**, 5569–5574 (2007).
47. Huang, C. *et al.* The structure of a human p110alpha/p85alpha complex elucidates the effects of oncogenic PI3Kalpha mutations. *Science* **318**, 1744–1748 (2007).
48. Dbouk, H. A. *et al.* G protein-coupled receptor-mediated activation of p110β by Gβγ is required for cellular transformation and invasiveness. *Sci Signal* **5**, ra89–ra89 (2012).
49. Dornan, G. L. *et al.* Conformational disruption of PI3Kδ regulation by immunodeficiency mutations in PIK3CD and PIK3R1. *Proc. Natl. Acad. Sci. U.S.A.* **114**, 1982–1987 (2017).
50. Takeda, A. J. *et al.* Novel PIK3CD mutations affecting N-terminal residues of p110δ cause activated PI3Kδ syndrome (APDS) in humans. *J. Allergy Clin. Immunol.* **140**, 1152-1156.e10 (2017).
51. Vallejo-Díaz, J., Chagoyen, M., Olazabal-Morán, M., González-García, A. & Carrera, A. C. The Opposing Roles of PIK3R1/p85α and PIK3R2/p85β in Cancer. *Trends in Cancer* **5**, 233–244 (2019).
52. Zhang, X. *et al.* Structure of lipid kinase p110β/p85β elucidates an unusual SH2-domain-mediated inhibitory mechanism. *Mol Cell* **41**, 567–578 (2011).
53. Zhang, M., Jang, H. & Nussinov, R. Structural Features that Distinguish Inactive and Active PI3K Lipid Kinases. *J Mol Biol* **432**, 5849–5859 (2020).
54. Carson, J. D. *et al.* Effects of oncogenic p110alpha subunit mutations on the lipid kinase activity of phosphoinositide 3-kinase. *Biochem. J.* **409**, 519–524 (2008).
55. Swaney, D. L. *et al.* A protein network map of head and neck cancer reveals PIK3CA mutant drug sensitivity. *Science* **374**, eabf2911 (2021).
56. Song, K. W. *et al.* RTK-Dependent Inducible Degradation of Mutant PI3Ka Drives GDC-0077 (Inavolisib) Efficacy. *Cancer Discov* (2021) doi:10.1158/2159-8290.CD-21-0072.
57. Dobbs, J. M., Jenkins, M. L. & Burke, J. E. Escherichia coli and Sf9 Contaminant Databases to Increase Efficiency of Tandem Mass Spectrometry Peptide Identification in Structural Mass Spectrometry Experiments. *J Am Soc Mass Spectrom* **31**, 2202–2209 (2020).
58. Perez-Riverol, Y. *et al.* The PRIDE database and related tools and resources in 2019: improving support for quantification data. *Nucleic Acids Res.* **47**, D442–D450 (2019).

Supplementary Figures + Tables for

Oncogenic mutations of *PIK3CA* lead to increased membrane recruitment driven by reorientation of the ABD, p85 and C-terminus

Harish Ranga-Prasad[1], Meredith L Jenkins[1], Matthew AH Parson[1], Manoj K Rathinaswamy[1], John E Burke[1,3%]

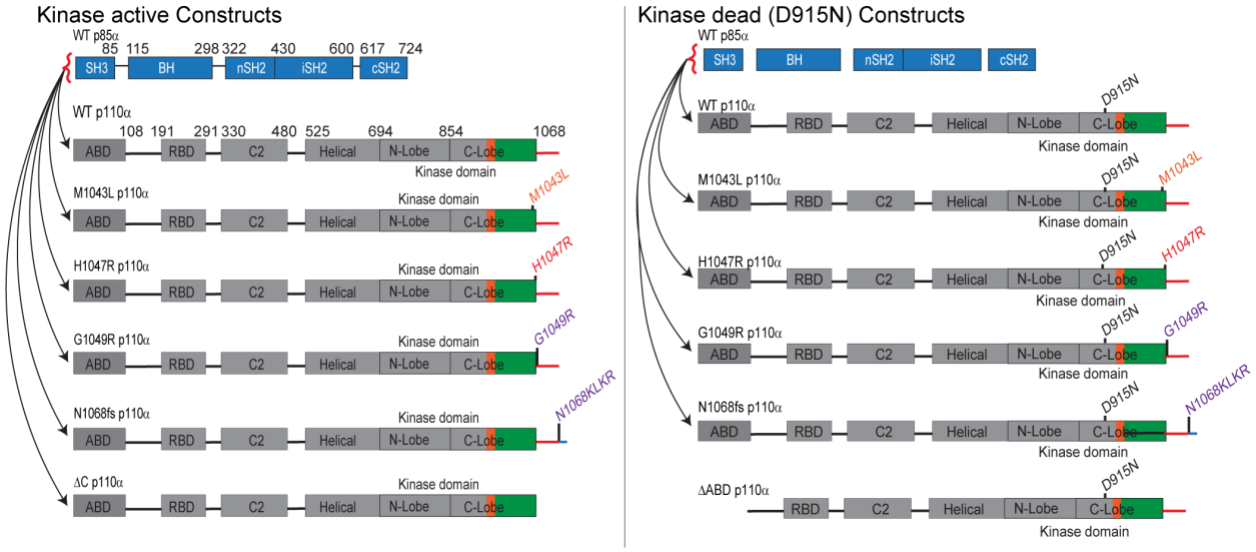

Fig S1- List of p110α and p85α constructs used.

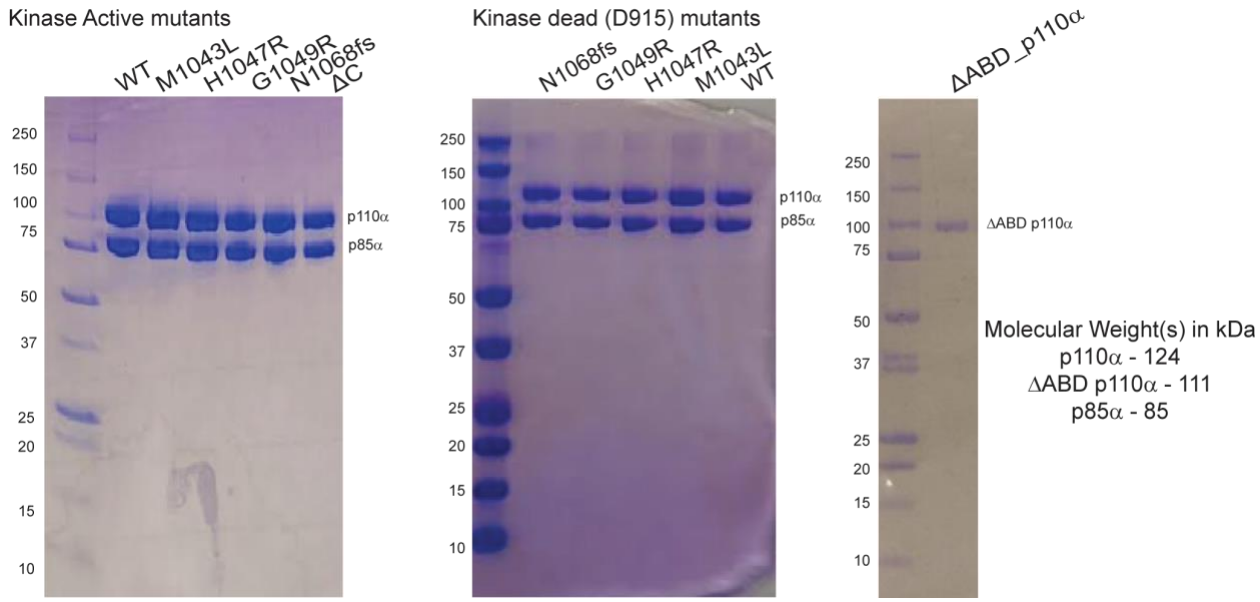

Fig S2. SDS PAGE gel images of all p110α constructs used in this study

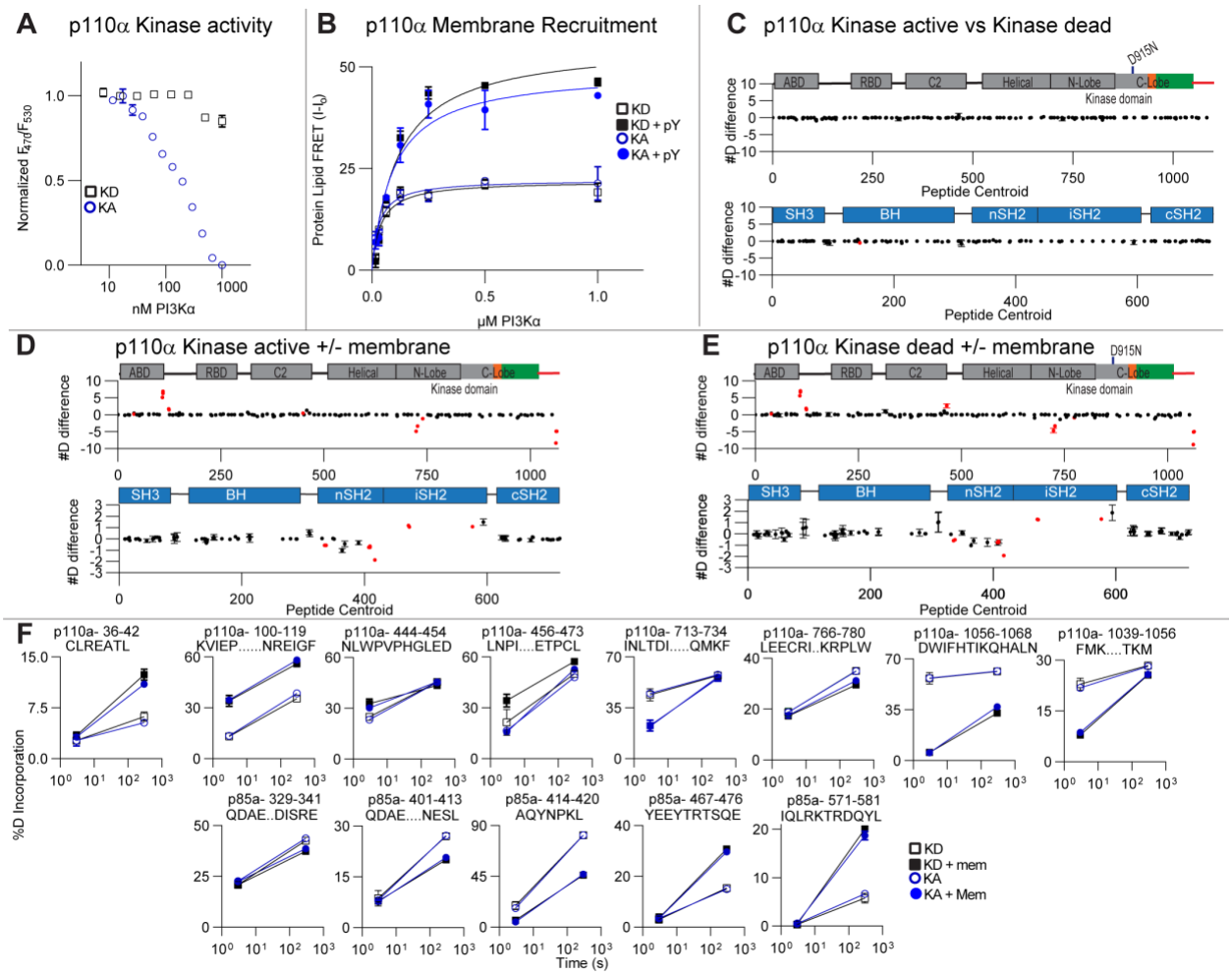

Fig S3 Comparison between kinase active (KA) and kinase dead (KD) p110α

A. Lipid kinase assay performed with kinase active and kinase dead p110α constructs under basal state. Experiments were performed with1 μM ATP, 0.4 X 10^{-3} to 0.8 μM PI3K, and 1 mg/ml of PIP_2/PS/PE lipids (5% PIP_2, 30% PS, 65% PE). Error bars shown are SD (n=3)

B. Protein-Lipid FRET assay performed with kinase active and kinase dead p110α constructs under basal and pY activated states on liposomes containing 5% PIP_2, 10% Dansyl PS, 25 % PS, 65% PE. Experiments were carried out at saturating concentrations of PI3K concentrations ranging from 0.015 to 1μM, 1μM pY, and 33.33 μg/ml of lipid vesicles (error bars are S.D., n=3).

(C-E). The #D difference in deuterium incorporation for p110α and p85α in each experiment, with each point representing a single peptide, with error as SD (n=3). comparing the following conditions: **C.** p110α/p85α WT kinase active vs kinase dead. **D.** WT kinase active in solution and membrane. **E.** WT

kinase dead in solution and membrane. Peptides in p110α and p85α that showed significant differences in HDX upon binding to 100 nm extruded 5% PIP_2/PS/PE vesicles are colored in red (greater than 0.4 Da and 5% difference at any timepoint, with a two tailed t-test $p<0.01$).

F. %D graphs for a selection of peptides comparing WT kinase active vs Kinase dead under pY active state and membrane bound state. Full HDX-MS data available in source data.

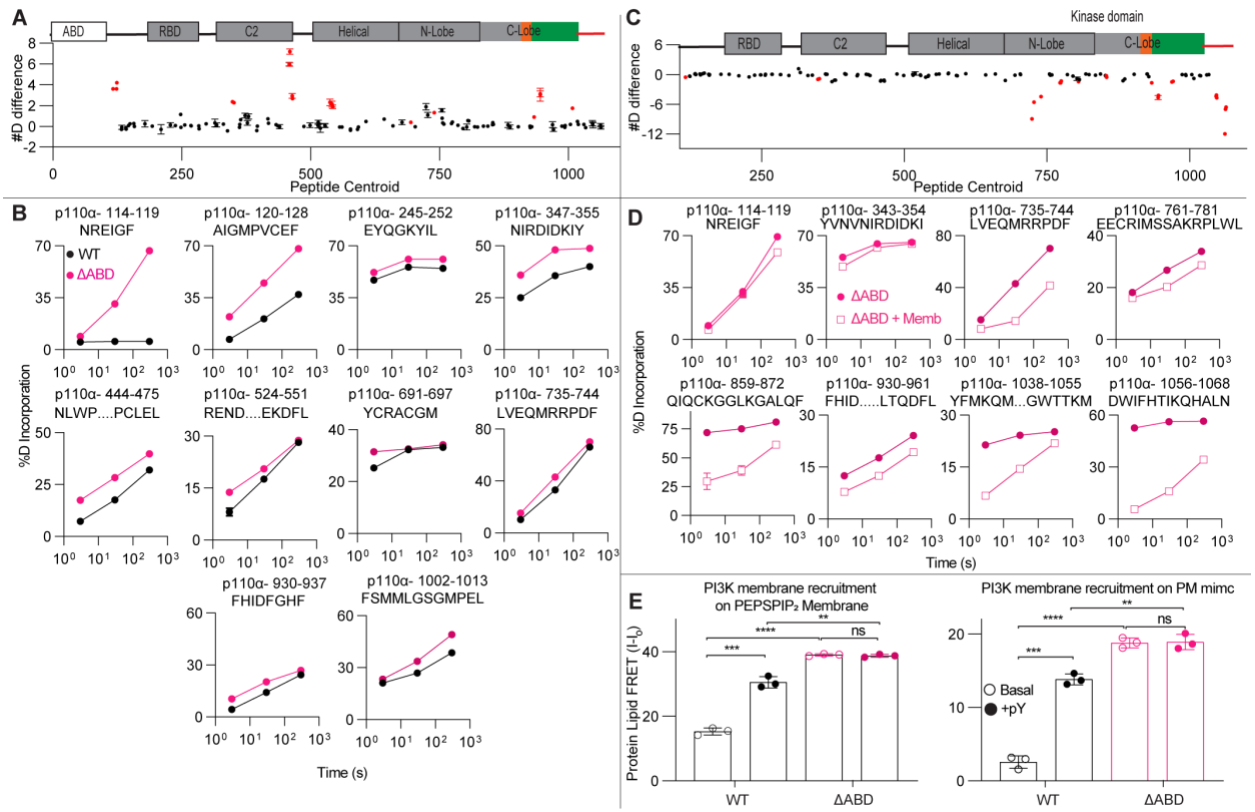

Fig S4 HDX-MS differences for experiments done with ΔABD

A. The #D difference in deuterium incorporation for p110α between ΔABD and full-length p110α/p85α complex with error as SD (n=3). Peptides in p110α that showed significant differences in HDX are colored in red (greater than 0.4 Da and 5% difference at any timepoint, with a two tailed t-test p<0.01).

B. %D graphs for a selection of peptides comparing ΔABD and full-length p110α/p85α with error as SD (n=3). Full HDX-MS data available in source data.

C. The #D difference in deuterium incorporation for ΔABD upon binding 5% PIP_2 membranes with error as SD (n=3). Peptides in p110α that showed significant differences in HDX are colored in red (greater than 0.4 Da and 5% difference at any timepoint, with a two tailed t-test p<0.01).

D. %D graphs for a selection of peptides comparing for ΔABD in the presence and absence of 5% PIP_2 membranes with error as SD (n=3).

E. Protein-Lipid FRET on PIP_2/PS/PE and PM mimic membranes. FRET assays were performed with saturating concentrations of PI3K (0.5 µM) and 33.33 µg of lipid (error bars are S.D., n=3). Two tailed p-values represented by the symbols as follows: ****<0.0001, ***<0.001; **<0.01; *<0.05; n.s.>0.05.

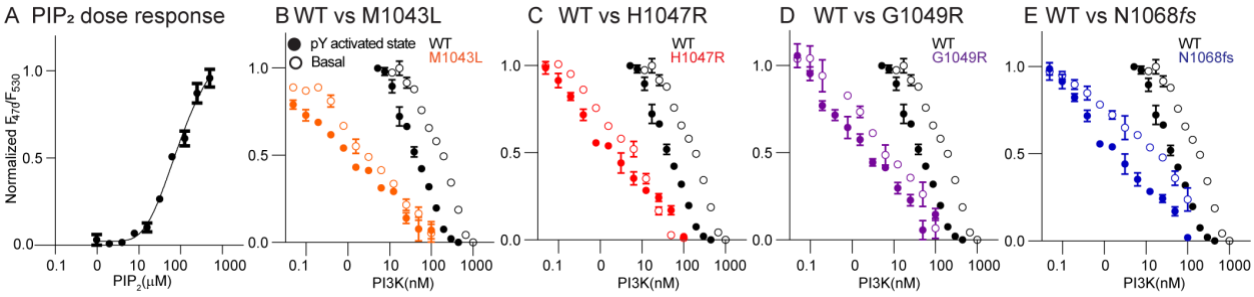

Fig S5 Kinase assays comparison between WT and mutants under basal and pY activated state

A. Dose response with 500nM PIP_2 sensor and 0 to 2.5 mg/ml of PIP_2/PS/PE (5% PIP2, 30% PS, 65% PE) liposomes.

B-E. Lipid kinase assay comparing basal and pY activated states of WT vs (B) M1043L (C) H1047R (D) G1049R and (E) N1068fs Experiments were performed with 500nM PIP_2 sensor, 1 μM ATP, 1 μM pY, 1 mg/ml of PIP_2/PS/PE liposomes and 0.4 X 10-3 to 0.8 μM PI3K. (Error bars are SD, n=3).

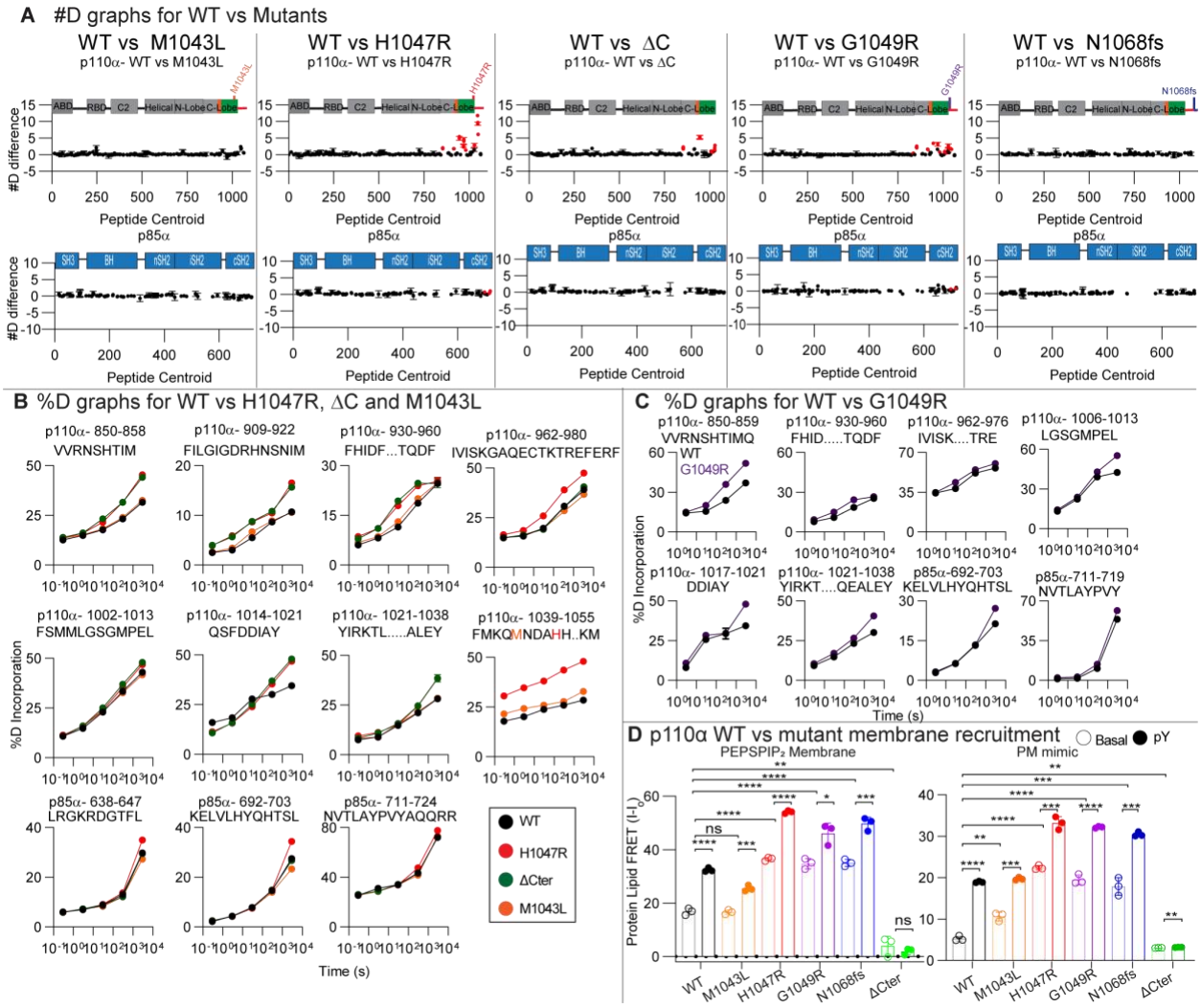

Fig S6 Source data for experiments comparing WT and different c-terminal mutants

A. The #D difference in deuterium incorporation for p110α and p85α in between WT and the indicated p110α mutant or deletion with error as SD (n=3). Peptides in p110α and p85α that showed significant differences in HDX are colored in red (greater than 0.4 Da and 5% difference at any timepoint, with a two tailed t-test p<0.01).

Peptide graphs for HDX differences between WT and mutants showing changes in both p110α and p85α

B-C. % D graphs for a selection of peptides showing significant differences between and WT and mutants. Full HDX-MS data available in the source data.

D. Protein-Lipid FRET assay performed with different p110α constructs under basal and pY activated states on PM mimic liposomes (5% PIP_2, 10% Dansyl PS, 15 % PS, 40% PE, 10% cholesterol, 15% PC and 5%

SM) and 5% PIP_2, 10% Dansyl PS, 25 % PS, 65% PE liposomes. Experiments were carried out at saturating concentrations of PI3K (1μM) and 33.33 μg/ml of lipid vesicles (error bars are S.D., n=3). Two tailed p-values represented by the symbols as follows: ****<0.0001, ***<0.001; **<0.01; *<0.05; n.s.>0.05.

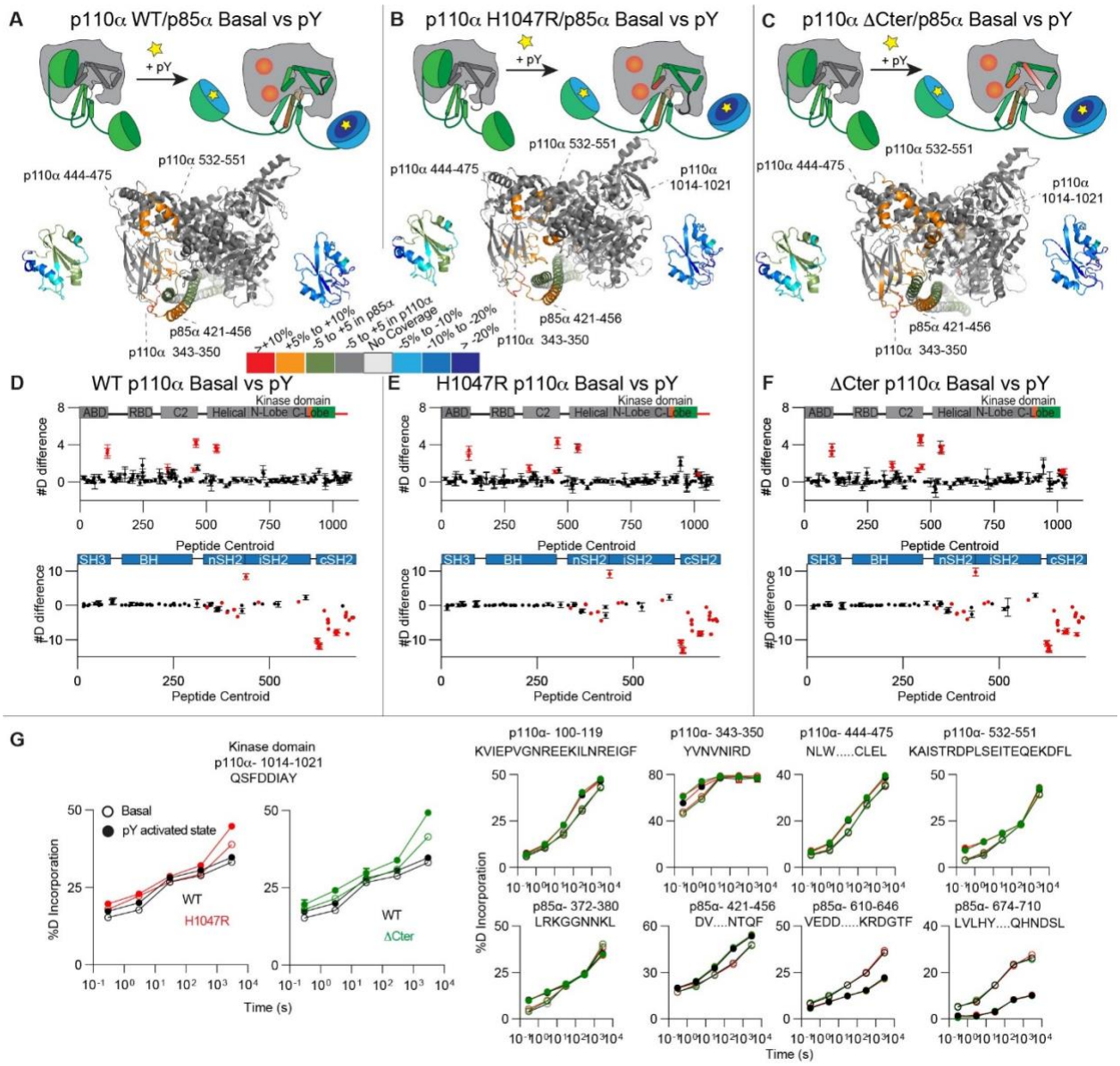

Fig S7. Addition of pY leads to increased exposure in the kinase domain.

A-C. HDX-MS comparing basal and pY activated states of (**A**) WT (**B**) H1047R and (**C**) the ΔC-terminus. The differences with H1047R were mapped onto p110α/iSH2-nSh2 (PDB: 3HHM) and cSH2 (2Y3A). The differences between WT and ΔCter were mapped onto p110α/iSH2-nSH2 (PDB: 4OVU) and nSH2 (2Y3A)

D-F. The #D difference in deuterium incorporation for p110α and p85α upon pY binding for the indicated p110α mutant or deletion with error as SD (n=3). Peptides in p110α and p85α that showed significant differences in HDX are colored in red (greater than 0.4 Da and 5% difference at any timepoint, with a two tailed t-test $p<0.01$).

G. %D graphs for a selection of peptides with differences in exchange, with all HDX-MS data available in the source data.

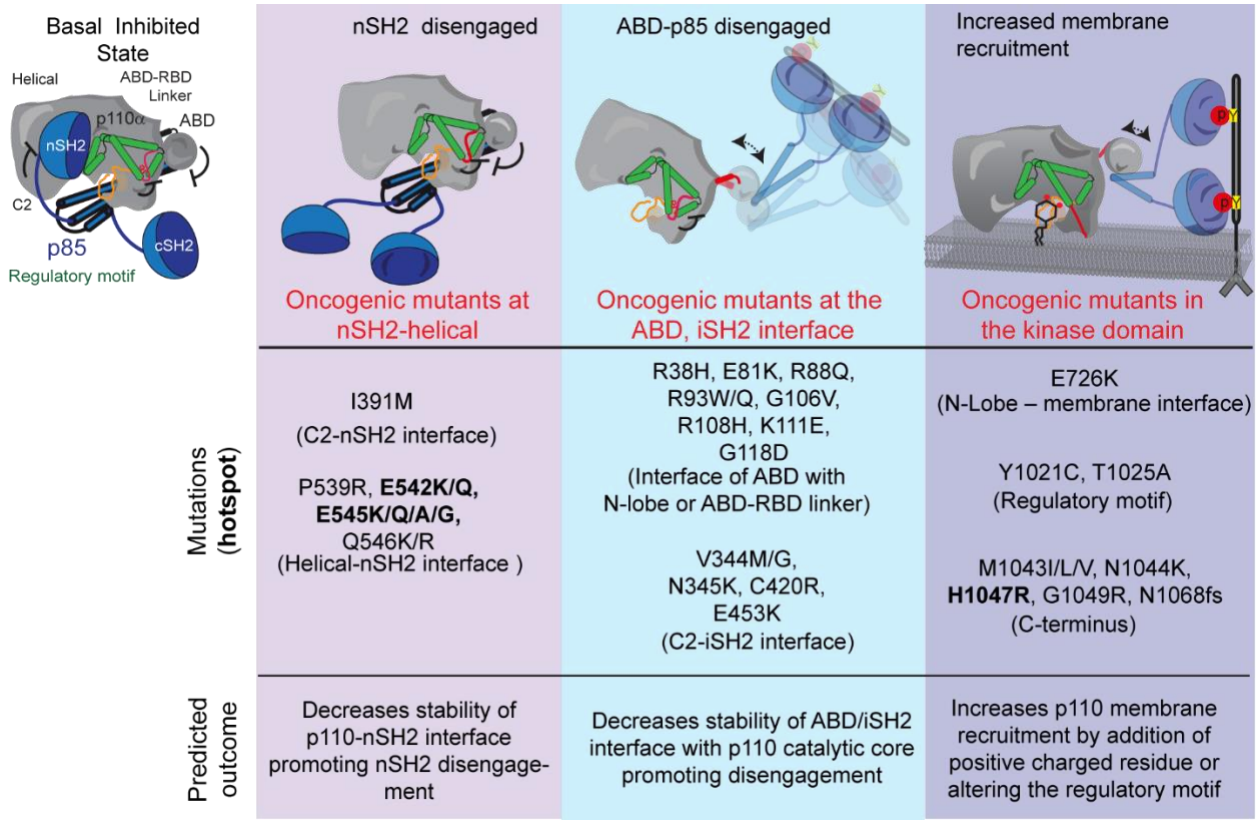

Figure S8: Predicted molecular mechanism of activation for various PIK3CA mutations. Mutations at the nSH2 interface/helical domain lead to disengagement of the nSH2 while the mutations at the ABD/C2 promote disengagement of ABD-p85 from the catalytic core. Mutations at the kinase domain promote membrane recruitment either by addition of positively charged residue at the membrane binding interface (E726K) or alter the regulatory motif.

Table S1- HDX-MS processing details

Experiment	Comparing WT PI3K and Delta ABD PI3K. HDX Stats table for data shown in Figure 2 and Figure 3.		
Data set	WT	Delta ABD	Delta ABD + Memb
HDX reaction details	%D_2O=69% $pH_{(read)}$=7.5 Temp=18ºC	%D_2O=69% $pH_{(read)}$=7.5 Temp=18ºC	%D_2O=69% $pH_{(read)}$=7.5 Temp=18ºC
HDX time course (seconds)	3s, 30s, 300s	3s, 30s, 300s	3s, 30s, 300s
HDX controls	N/A	N/A	N/A
Back-exchange	No correction, deuterium levels are relative	No correction, deuterium levels are relative	No correction, deuterium levels are relative
Replicates	3	3	3
Protein	p110a		
Number of peptides	125	125	125
Sequence coverage	89.9%	89.9%	89.9%
Average peptide /redundancy	Length= 13.9 Redundancy= 1.8	Length= 13.9 Redundancy= 1.8	Length= 13.9 Redundancy= 1.8
Repeatability	Average StDev= 0.6%	Average StDev=0.4%	Average StDev=0.6%

Experiment	Comparing basal PI3K WT vs mutants (H1047R, M1043L and Delta C) and in the presence of pY with H1047R and Delta C. HDX Stats table for data shown in Figure 5A, Figure 5C, Figure 5D and Figure S7

Data set	WT	WT+pY	H1047R	H1047R + pY	M1043L	Delta C	Delta C + pY
HDX reaction details	%D_2O=75% $pH_{(read)}$=7.5 Temp=18ºC	%D_2O=75% $pH_{(read)}$=7.5 Temp=18ºC	%D_2O=75% $pH_{(read)}$=7.5 Temp=18ºC	%D_2O=75% $pH_{(read)}$=7.5 Temp=18ºC	%D_2O=75% $pH_{(read)}$=7.5 Temp=18ºC	%D_2O=75% $pH_{(read)}$=7.5 Temp=18ºC	%D_2O=75% $pH_{(read)}$=7.5 Temp=18ºC
HDX time course (seconds)	3s, 30s, 300s, 3000s at 18ºC 3s at 0 ºC	3s, 30s, 300s, 3000s at 18ºC 3s at 0 ºC	3s, 30s, 300s, 3000s at 18ºC 3s at 0 ºC	3s, 30s, 300s, 3000s at 18ºC 3s at 0 ºC	3s, 30s, 300s, 3000s at 18ºC 3s at 0 ºC	3s, 30s, 300s, 3000s at 18ºC 3s at 0 ºC	3s, 30s, 300s, 3000s at 18ºC 3s at 0 ºC
HDX controls	N/A	N/A	N/A	N/A	N/A	N/A	N/A
Back-exchange	No correction deuterium levels are relative	No correction deuterium levels are relative	No correction deuterium levels are relative	No correction deuterium levels are relative	No correction deuterium levels are relative	No correction deuterium levels are relative	No correction deuterium levels are relative
Replicates	3	3	3	3	3	3	3
Significant differences in HDX	>5% and >0.4 Da and unpaired t-test ≤0.01	>5% and >0.4 Da and unpaired t-test ≤0.01	>5% and >0.4 Da and unpaired t-test ≤0.01	>5% and >0.4 Da and unpaired t-test ≤0.01	>5% and >0.4 Da and unpaired t-test ≤0.01	>5% and >0.4 Da and unpaired t-test ≤0.01	>5% and >0.4 Da and unpaired t-test ≤0.01
Protein							
Number peptides	171	171	170	170	169	164	164
Sequence coverage	95.8%	95.8%	95.8%	95.8%	95.8%	95.8%	95.8%
Average peptide /redundancy	Length= 13.7 Redundancy = 2.1	Length= 13.7 Redundancy = 2.1	Length= 13.7 Redundancy = 2.1	Length= 13.7 Redundancy = 2.1	Length= 13.7 Redundancy = 2.1	Length= 13.7 Redundancy = 2.1	Length= 13.7 Redundancy = 2.1
Repeatability	Average StDev=0.5%	Average StDev=0.5%	Average StDev=0.6%	Average StDev=0.5%	Average StDev=0.5%	Average StDev=0.5%	Average StDev=0.5%
Protein							
Number peptides	117	117	117	117	117	117	117
Sequence coverage	90.3%	90.3%	90.3%	90.3%	90.3%	90.3%	90.3%
Average peptide /redundancy	Length= 16.3 Redundancy = 2.6	Length= 16.3 Redundancy = 2.6	Length= 16.3 Redundancy = 2.6	Length= 16.3 Redundancy = 2.6	Length= 16.3 Redundancy = 2.6	Length= 16.3 Redundancy = 2.6	Length= 16.3 Redundancy = 2.6
Repeatability	Average StDev=0.5%	Average StDev=0.6%	Average StDev=0.6%	Average StDev=0.5%	Average StDev=0.6%	Average StDev=0.6%	Average StDev=0.6%

Experiment	Comparing Kinase Active PI3K and G1049R PI3K. HDX Stats table for data shown in Figure 5B and Figure 5F	
Data set	WT	G1049R

HDX reaction details	%D_2O=76% $pH_{(read)}$=7.5 Temp=18ºC	%D_2O=76% $pH_{(read)}$=7.5 Temp=18ºC
HDX time course (seconds)	3s, 30s, 300s, 3000s	3s, 30s, 300s, 3000s
HDX controls	N/A	N/A
Back-exchange	No correction, deuterium levels are relative	No correction, deuterium levels are relative
Replicates	3	3
Significant differences in HDX	>5% and >0.4 Da and unpaired t-test ≤0.01	>5% and >0.4 Da and unpaired t-test ≤0.01
Protein	p110a	
Number of peptides	169	169
Sequence coverage	95.2%	95.2%
Average peptide /redundancy	Length=13.7 Redundancy=2.1	Length=13.7 Redundancy=2.1
Repeatability	Average StDev=0.6%	Average StDev=0.5%
Protein	p85	
Number of peptides	114	114
Sequence coverage	89%	89%
Average peptide /redundancy	Length=16.4 Redundancy=2.5	Length=16.4 Redundancy=2.5
Repeatability	Average StDev=0.6%	Average StDev=0.5%

Experiment	Comparing Kinase Active PI3K and Frameshift. HDX Stats table for data shown in Figure 5E	
Data set	WT	Frameshift
HDX reaction details	%D_2O=81% $pH_{(read)}$=7.5 Temp=18ºC	%D_2O=81% $pH_{(read)}$=7.5 Temp=18ºC
HDX time course (seconds)	3s, 30s, 300s, 3000s	3s, 30s, 300s, 3000s
HDX controls	N/A	N/A
Back-exchange	No correction, deuterium levels are relative	No correction, deuterium levels are relative
Replicates	3	3
Significant differences in HDX	>5% and >0.4 Da and unpaired t-test ≤0.01	>5% and >0.4 Da and unpaired t-test ≤0.01
Protein	p110a	
Number of peptides	141	139
Sequence coverage	84.7%	84.7%
Average peptide /redundancy	Length= 13.7 Redundancy= 1.6	Length= 13.7 Redundancy= 1.6
Repeatability	Average StDev=0.9%	Average StDev=0.7%
Protein	p85	
Number of peptides	180	180
Sequence coverage	79%	79%
Average peptide /redundancy	Length= 16 Redundancy= 2.6	Length= 16 Redundancy= 2.6
Repeatability	Average StDev=0.9%	Average StDev=0.6%

Experiment	Comparing Kinase Active PI3K and Kinase Dead (KD) PI3K. HDX Stats table for data shown in Supplemental Figure 3			
Data set	WT	WT+memb	KD	KD + Memb
HDX reaction details	%D_2O=72% $pH_{(read)}$=7.5 Temp=18ºC	%D_2O=72% $pH_{(read)}$=7.5 Temp=18ºC	%D_2O=72% $pH_{(read)}$=7.5 Temp=18ºC	%D_2O=72% $pH_{(read)}$=7.5 Temp=18ºC
HDX time course (seconds)	3s, 300s	3s, 300s	3s, 300s	3s, 300s
HDX controls	N/A	N/A	N/A	N/A
Back-exchange	No correction, deuterium levels are relative	No correction, deuterium levels are relative	No correction, deuterium levels are relative	No correction, deuterium levels are relative
Replicates	3	3	3	3
Significant differences in HDX	>5% and >0.4 Da and unpaired t-test ≤0.01	>5% and >0.4 Da and unpaired t-test ≤0.01	>5% and >0.4 Da and unpaired t-test ≤0.01	>5% and >0.4 Da and unpaired t-test ≤0.01
Protein	p110a			
Number of peptides	133	133	133	133
Sequence coverage	84.9%	84.9%	84.9%	84.9%
Average peptide /redundancy	Length=13.1 Redundancy=1.5	Length=13.1 Redundancy=1.5	Length=13.1 Redundancy=1.5	Length=13.1 Redundancy=1.5
Repeatability	Average StDev=0.7	Average StDev=0.7	Average StDev=1.1%	Average StDev=1.3%
Protein	p85			
Number of peptides	81	81	81	81
Sequence coverage	71.4%	71.4%	71.4%	71.4%
Average peptide /redundancy	Length=15.1 Redundancy=1.6	Length=15.1 Redundancy=1.6	Length=15.1 Redundancy=1.6	Length=15.1 Redundancy=1.6
Repeatability	Average StDev=0.7	Average StDev=0.6%	Average StDev=1.4%	Average StDev=1%